Thermal Equilibrium of the Atmosphere with a Convective Adjustment

SYUKURO MANABE AND ROBERT F. STRICKLER

General Circulation Research Laboratory, U. S. Weather Bureau, Washington, D. C.

(Manuscript received 19 December 1963, in revised form 13 April 1964)

ABSTRACT

The states of thermal equilibrium (incorporating an adjustment of super-adiabatic stratification) as well as that of pure radiative equilibrium of the atmosphere are computed as the asymptotic steady state approached in an initial value problem. Recent measurements of absorptivities obtained for a wide range of pressure are used, and the scheme of computation is sufficiently general to include the effect of several layers of clouds.

The atmosphere in thermal equilibrium has an isothermal lower stratosphere and an inversion in the upper stratosphere which are features observed in middle latitudes. The role of various gaseous absorbers (i.e., water vapor, carbon dioxide, and ozone), as well as the role of the clouds, is investigated by computing thermal equilibrium with and without one or two of these elements. The existence of ozone has very little effect on the equilibrium temperature of the earth's surface but a very important effect on the temperature throughout the stratosphere; the absorption of solar radiation by ozone in the upper and middle stratosphere, in addition to maintaining the warm temperature in that region, appears also to be necessary for the maintenance of the isothermal layer or slight inversion just above the tropopause. The thermal equilibrium state in the absence of solar insolation is computed by setting the temperature of the earth's surface at the observed polar value. In this case, the stratospheric temperature decreases monotonically with increasing altitude, whereas the corresponding state of pure radiative equilibrium has an inversion just above the level of the tropopause.

A series of thermal equilibriums is computed for the distributions of absorbers typical of different latitudes. According to these results, the latitudinal variation of the distributions of ozone and water vapor may be partly responsible for the latitudinal variation of the thickness of the isothermal part of the stratosphere. Finally, the state of local radiative equilibrium of the stratosphere overlying a troposphere with the observed distribution of temperature is computed for each season and latitude. In the upper stratosphere of the winter hemisphere, a large latitudinal temperature gradient appears at the latitude of the polar-night jet stream, while in the upper statosphere of the summer hemisphere, the equilibrium temperature varies little with latitude. These features are consistent with the observed atmosphere. However, the computations predict an extremely cold polar night temperature in the upper stratosphere and a latitudinal decrease (toward the cold pole) of equilibrium temperature in the middle or lower stratosphere for winter and fall. This disagrees with observation, and suggests that explicit introduction of the dynamics of large scale motion is necessary.

CONTENTS

1. Introduction

The study of the thermal equilibrium of the atmosphere might serve the following purposes:

1. Formulation and the test of a method to incorporate radiative transfer into an advanced general circulation model of the atmosphere.
2. Determination of the role of various atmospheric absorbers in maintaining the existing thermal structure of the atmosphere. For example, it might help one to understand how the troposphere is built up and why the tropopause occurs where it is observed.
3. Determination of the role of various atmospheric absorbers in maintaining the observed climate at the earth's surface.

Study of the radiative equilibrium of a non-gray atmosphere has been carried out by Gowan (1928), Goody (1949), King (1952, 1956), Yamamoto (1955) and others. In order to evaluate these theories from a more geophysical viewpoint and to prepare for the incorporation of a realistic radiative model into a general circulation model, Möller and Manabe (1961) also attempted to study the radiative equilibrium of a non-gray atmosphere. (Hereafter, this paper will be referred to as "B.") In (B), the absorbers taken into consideration were water vapor, carbon dioxide and ozone. Although this study of pure radiative equilibrium gave some indication of the role of these absorbing gases in maintaining the existing thermal structure of the atmosphere, the conclusions must be accepted with some reservations because the equilibrium temperature of the upper troposphere turned out to be much lower than the observed value. This is most likely because of the complete disregard of atmospheric motion in the computations. For the same reason, the temperature of the earth's surface computed in (B) was much warmer than the observed value. To overcome this defect, Manabe and Möller (1961) in another study of this same problem, hereafter designated as "A", computed the radiative equilibrium of the atmosphere with a fixed surface temperature close to the observed value. As one might expect, the temperature of the upper troposphere again turned out to be very low compared to observed values. In order to overcome this difficulty, it would be desirable to construct a general atmospheric model which would include all the important dynamical processes as well as the process of radiative transfer. Before doing this, however, it is desirable to introduce the very simple process of a *convective adjustment* to approximate the upward heat transfer by atmospheric motions. The actual procedure used in the present calculations is continually to make an adjustment to a given critical lapse rate of temperature whenever, in the course of approaching the final steady state, the lapse rate tends to exceed the critical rate. It is expected that this process of convective adjustment will transfer heat energy from the earth's surface into the lower and upper troposphere and thereby permit more realistic temperatures to occur throughout the troposphere. The temperature of the earth's surface is essentially determined by the requirement of no net radiation at the top of the atmosphere, the constraint of a critical lapse rate for convection, and the assumption of no heat storage at the earth's surface.

Improved experimental data and our numerical computation of absorptivity over a wide range of pressure permitted considerable refinement of the present calculations of radiative flux compared to those of the previous study (A).

2. Thermal equilibrium

a. Pure radiative equilibrium. In order to prepare for the study of thermal equilibrium with convective adjustment, calculations were first performed for the simple case of purely radiative equilibrium in which pure radiative equilibrium was approached as an asymptotic steady state of an initial value problem. Although the rate of convergence of this method might be slower than that of a more efficiently designed iterative method for determination of the equilibrium state, this scheme was chosen so that we could study the computational stability characteristics of the time dependent model. This type of information is important for the incorporation of the present scheme of radiative calculation into a general circulation model of the atmosphere.

The state of pure radiative equilibrium was approached by the following method of numerical integration:

$$T^{\tau+1}=T^{\tau}+\left(\frac{\partial T}{\partial t}\right)^{\tau}\cdot\Delta t, \tag{1}$$

where T^{τ} is the temperature at the τ-th time step, and Δt is the time interval. As mentioned in (A), forward differencing was used. The largest allowable time interval which guarantees computational stability was obtained by trial and error. Equilibrium was considered to have been reached when the temperature change $T^{\tau+1}-T^{\tau}$ at each layer was less than a small value, δ.

Other requirements for pure radiative equilibrium are:

1) At the earth's surface, the net upward flux of long wave radiation is equal to the net downward flux of solar radiation.
2) At the top of the atmosphere, the net upward flux of long wave radiation is equal to the net downward solar radiation. The asymptotic state of radiative equilibrium is approached when this condition is approximately satisfied.

The first requirement guarantees the radiative equilibrium of the earth's surface and the second requirement guarantees the radiative equilibrium of both the atmosphere and the earth as a whole. In the course of the computation, the temperature jump which theo-

retically exists between the atmosphere and the earth's surface is smoothed out by the vertical finite difference representation of the equations of radiative transfer. Fortunately, the magnitude of the theoretical temperature jump is much smaller than would be the case if a gray assumption were made for the absorption and emission of radiation. This is due partly to the very strong absorption near the line centers, and also to the upward radiation from the earth's surface through the nearly transparent regions in the line wings and through the window region of water vapor, which compensates for most of the net downward solar radiation at the earth's surface. Accordingly, the condition of no heat storage at the earth's surface could be satisfied radiatively by a temperature jump which is much smaller than that for the gray absorber. In the previous study (B), this temperature jump at the surface turned out to be less than 1 deg, depending upon the amount of water vapor and other parameters. Thus, the neglect of the temperature jump would not produce a serious error in the results.

b. Thermal equilibrium with convective adjustment. The procedure of convective adjustment is to adjust the lapse rate to the critical lapse rate whenever the critical lapse rate is exceeded in the course of the numerical integration of the initial value problem. The observed tropospheric lapse rate of temperature is approximately 6.5 deg km^{-1}. The explanation for this fact is rather complicated. It is essentially the result of a balance between (*a*) the stabilizing effect of upward heat transport in moist and dry convection on both small and large scales and (*b*), the destabilizing effect of radiative transfer. Instead of exploring the problem of the tropospheric lapse rate in detail, we here accept this as an observed fact and regard it as a critical lapse rate for convection.

The requirements for "thermal equilibrium" are then somewhat different from those of the pure radiative case. In the final state:

1) At the top of the atmosphere, the net incoming solar radiation should be equal to the net outgoing long wave radiation.
2) At the earth's surface, the excess of net downward solar radiation over net upward long wave radiation should equal the net integrated radiative cooling of the atmosphere. (This implies that at the earth's surface a balance exists between the net gain of energy by radiation and the loss of heat by convective transfer into the atmosphere.)
3) Wherever the lapse rate is subcritical, the condition of local radiative equilibrium is satisfied.

The following numerical procedures were used.

1) In a convective layer (a layer which without the adjustment would have a super-critical lapse rate) which is in contact with the earth's surface, the net rate of temperature change, $(\partial T/\partial t)_{\text{NET}}$, is determined to be such that it satisfies the following relations.[1]

$$(\partial T/\partial z)^{\tau+1}=(\text{critical lapse rate}), \tag{2}$$

where

$$T^{\tau+1}=T^{\tau}+(\partial T/\partial t)_{\text{NET}}{}^{\tau}\cdot\Delta t \tag{3}$$

and

$$\frac{C_p}{g}\int_{P_{cT}}^{P_*}\left(\frac{\partial T}{\partial t}\right)_{\text{NET}}^{\tau}dp =\frac{C_p}{g}\int_{P_{cT}}^{P_*}\left(\frac{\partial T}{\partial t}\right)_{\text{RAD}}^{\tau}dp+(-F_0{}^{\tau}+S_0), \tag{4}$$

where $(\partial T/\partial t)_{\text{RAD}}$ is the radiative temperature change. F_0 and S_0 are the net upward flux of long wave radiation and the net downward flux of solar radiation at the earth's surface. P_* and P_{CT} are the pressures at the earth's surface and at the top of the convective layer, while g and C_p are the acceleration of gravity and the specific heat of air at constant pressure. Equation (4) assumes that the earth's surface gives away as much heat as it receives, and does not have any capacity of heat storage.

For a convective layer which is not in contact with the earth's surface, the following equation, rather than equation (4), should be satisfied, because in this case there is no convective heat exchange with the earth's surface.

$$\frac{C_p}{g}\int_{P_{cT}}^{P_{cB}}\left(\frac{\partial T}{\partial t}\right)_{\text{NET}}^{\tau}dp=\frac{C_p}{g}\int_{P_{cT}}^{P_{cB}}\left(\frac{\partial T}{\partial t}\right)_{\text{RAD}}^{\tau}dp, \tag{5a}$$

where P_{cB} is the pressure at the bottom of the convective layer.

2) In a non-convective layer,

$$\left(\frac{\partial T}{\partial t}\right)_{\text{NET}}^{\tau}=\left(\frac{\partial T}{\partial t}\right)_{\text{RAD}}^{\tau}. \tag{5b}$$

3) In order to obtain the vertical distribution of the net temperature change which satisfies these relations, it is necessary to use an iteration procedure; at every time step the different layers into which the atmosphere is divided are scanned repeatedly until these conditions are satisfied.

c. Example of computation. Fig. 1 shows the approach to pure radiative equilibrium and thermal equilibrium,

[1] In order to stabilize the numerical computation, the temperature of the earth's surface at time step $\tau+1$ instead of τ was used in computating the upward flux of long wave radiation at the earth's surface. As we reach the final equilibrium which satisfies the requirements (1)–(3), this inconsistency should not cause any errors in the final equilibrium.

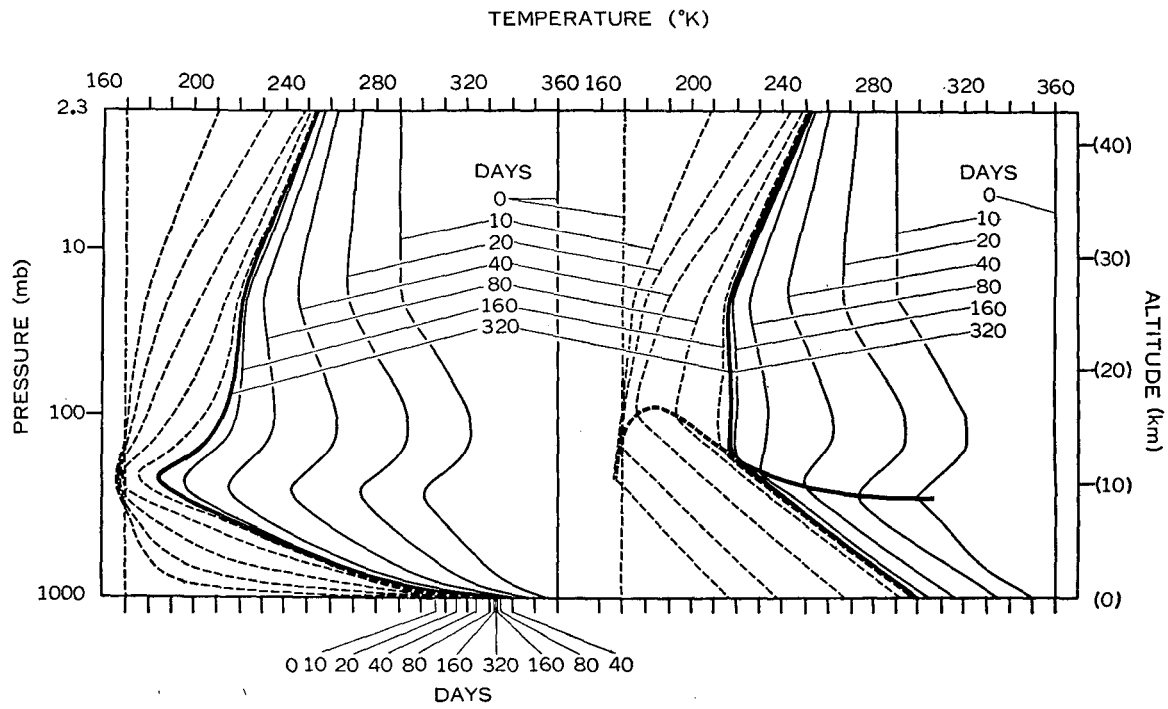

FIG. 1. The left and right hand sides of the figure, respectively, show the approach to states of pure radiative and thermal equilibrium. The solid and dashed lines show the approach from a warm and cold isothermal atmosphere.

from both initially warm and cold isothermal atmospheres. Refer to Section 4a for the amount of solar insolation and the distribution of gaseous absorbers which are adopted for these computations. Δt was 8 hr and the convergence criterion, δ, was 10^{-3} deg day^{-1}. It takes about one or two years to satisfy this criterion. At this time the relative magnitude of the difference between the net outgoing long wave radiation and the net incoming solar radiation is approximately 5×10^{-4} times either of these fluxes. The maximum difference in temperature between the two final states when approached from opposite directions is about 0.2 deg. These figures indicate that the final states may be regarded as steady states.[2]

3. Radiative temperature change of an atmosphere with clouds

a. Long wave radiation. As we stated in the introduction, one of the major purposes of our study is the construction of a model of radiative transfer simple enough to be incorporated into a general circulation model of the atmosphere. A comparison between the results obtained by the present method and those obtained by a more elaborate method suggests that the accuracy of the present method is sufficiently good for our purpose. [Refer to paper (A) and Appendix 3.] Although the basic framework for computing the infrared flux is similar to that explained in paper (A), it seems appropriate to describe it briefly here because of the various modifications we made.

As in (A), the absorption bands included in our scheme are: the rotation band and the 6.3 μ band of water vapor, the 15 μ band of CO_2 ,and the 9.6 μ band of O_3. The effect of overlapping between the 15 μ band of CO_2 and part of the rotation band of water vapor was incorporated. The resultant transmission for this overlapped range (550–800 cm^{-1}) was obtained as the product of two transmissivities [equation (18)]. We also generalize our scheme so we can take into consideration the effect of multilayer clouds. To illustrate we shall describe the calculation of the infrared flux in an atmosphere with clouds as shown in Fig. 2.

The influence of clouds on the infrared flux is estimated using the following assumptions:

1) High clouds (cirrus) are half black for atmospheric radiation.
2) The amount of sky covered by the overlapping of two or more cloud layers is equal to the product of the cloudiness at these layers. This is equivalent to assuming a uniform horizontal distribution of clouds in the sky.

[2] If one estimates the adjusted part of the lapse rate of thermal equilibrium shown on the right-hand side of Fig. 1 or in other figures by referring to the height scale at the right edge of the figure, one may not find it to be exactly 6.5 deg km^{-1} because this scale is applicable to the standard atmosphere and is not correct for an arbitrary distribution of temperature. The height scale should be used as an approximate reference only.

3) Within a cloud, the vertical distribution of radiative flux is assumed to be linear.

The net flux at level Z, F_Z, is defined as the difference between the total upward flux, $F_Z{}^{\uparrow}$, and the total downward flux, $F_Z{}^{\downarrow}$.

$$F_Z=F_Z{}^{\uparrow}-F_Z{}^{\downarrow}, \tag{6}$$

where

$$F_Z{}^{\downarrow}=C_1\cdot f_Z{}^{l_1}+(1-C_1)\cdot f_Z{}^{\infty} \tag{7a}$$

$$F_Z{}^{\uparrow}=C_2\cdot f_Z{}^{t_2}+C_3\cdot(1-C_2)\cdot f_Z{}^{t_3}+(1-C_2)(1-C_3)\cdot f_Z{}^{s}. \tag{7b}$$

In these equations C_n is the cloud amount for the n-th cloud, while $f_Z{}^{\infty}$ and $f_Z{}^{s}$ are the downward and upward clear sky fluxes at level Z, respectively. $C_1\cdot f_Z{}^{l_1}$ is the downward flux at level Z of radiation from the base of cloud 1. $C_2\cdot f_Z{}^{t_2}$ and $C_3\cdot f_Z{}^{t_3}$ are the upward fluxes from the tops of clouds 2 and 3, respectively. The amount of cirrus, C_1, is reduced by $\frac{1}{2}$ because of its partial transparency to long wave radiation. (This reduction was done for the computation of long wave radiation only.) Equations for the various radiative fluxes are derived as in (A) by solving the equation of radiative transfer using the boundary condition of no downward long wave radiation at the top of the atmosphere. The upward radiation at the earth's surface and at cloud tops, and the downward radiation at cloud bases is assumed to be equal to the blackbody radiation corresponding to the temperature of the ground or cloud surface. The equations for $f_Z{}^{l_1}$ and $f_Z{}^{\infty}$ are given as an example of infrared radiation flux equations.

$$f_Z{}^{l_1}=\pi B_{l1}-\int_{B_Z}^{B_{l1}}\tilde{\epsilon}_f{}^{W}(y^W,T)\pi dB-\int_{b_Z{}^C}^{b_{l1}{}^C}\tilde{\epsilon}_f{}^{C(W)}(y^C,T)\pi db^C-\int_{b_Z{}^0}^{b_{l1}{}^0}\tilde{\epsilon}_f{}^{0}(y^0,T)\pi db^0 \tag{8}$$

$$f_Z{}^{\infty}=\pi B_{\infty}\cdot\tilde{\epsilon}_f{}^{W}(y_{\infty}{}^W,T_{\infty})+\pi b_{\infty}{}^C\cdot\epsilon_f{}^{C(W)}(y_{\infty}{}^W,T)+\pi b_{\infty}{}^0\cdot\epsilon_f{}^{0}(y_{\infty}{}^0,T_{\infty})-\int_{B_Z}^{B_{\infty}}\tilde{\epsilon}_f{}^{W}(y^W,T)\pi dB-\int_{b_Z{}^C}^{b_{\infty}{}^C}\tilde{\epsilon}_f{}^{C(W)}(y^C,T)\pi db^C-\int_{b_Z{}^0}^{b_{\infty}{}^0}\tilde{\epsilon}_f{}^{o}(y^o,T)\pi db^o. \tag{9}$$

Most of the symbols adopted in these equations are consistent with the previous paper (A). However, we shall define them again for the convenience of the reader.

$$B(T)=\int_0^{\infty}B_{\nu}(T)d\nu \tag{10a}$$

$$b^G(T)=\int_{\nu_1{}^G}^{\nu_2{}^G}B_{\nu}(T)d\nu, \tag{10b}$$

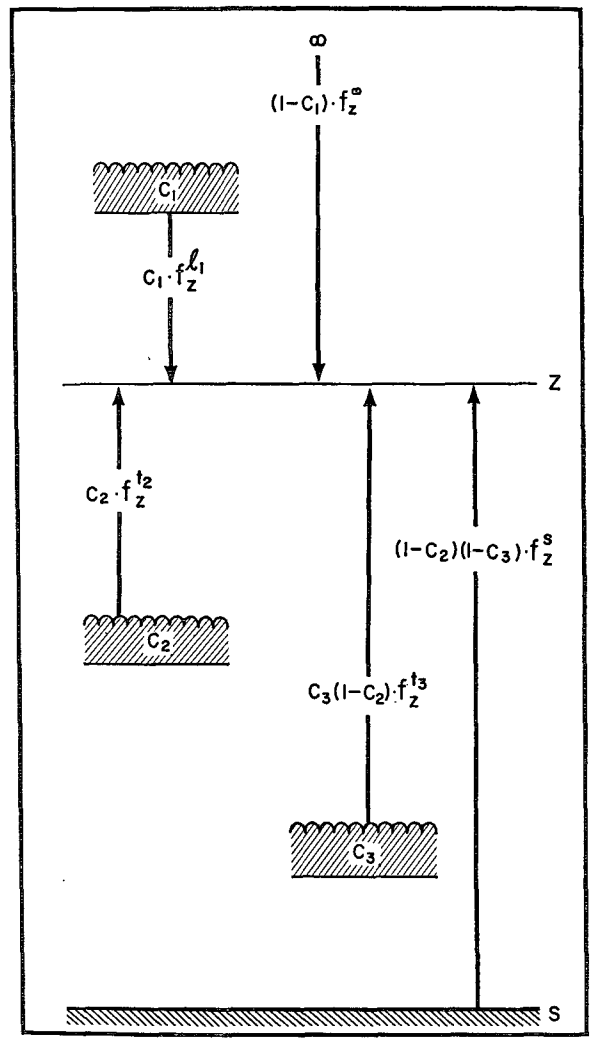

FIG. 2. Long wave radiation in an atmosphere with clouds.

where B_{ν} is the intensity of blackbody radiation at wave number ν, G stands for either C (carbon dioxide) or O (ozone), and $\nu_1{}^G$ and $\nu_2{}^G$ are the band limits of gas G. $B_Z=B(T_Z)$, $B_{\infty}=B(T_{\infty})$, $B(l_1)=B(T_{l_1})$, and $b^G(l_1)=b^G(T_{l_1})$.

$$y^G(B(T))=|u_r{}^G(T)-u_r{}^G(T_Z)| \tag{11a}$$

$$y_{\infty}{}^G=|u_r{}^G(T_{\infty})-u_r{}^G(T_Z)|, \tag{11b}$$

where $u_r{}^G(T_Z)$, for example, is the effective optical thickness of gas G between the earth's surface and level Z (where the temperature is T_Z). The slab emissivity and the mean slab absorptivity of water vapor are defined by

$$\epsilon_f{}^{W}(u,T)=\left[\int_0^{\infty}B_{\nu}(T)\cdot\{1-\tau_f(k_{\nu}{}^W\cdot u)\}d\nu\right]\Big/B(T) \tag{12}$$

and

$$\tilde{\epsilon}_f^W(u,T) = \left[\int_0^\infty \frac{dB_\nu(T)}{dT}\{1-\tau_f(k_\nu^W \cdot u)\}d\nu\right] \Big/ \frac{dB(T)}{dT}, \quad (13)$$

where τ_f is the slab transmissivity, and k_ν^W is the absorption coefficient of water vapor at wave number ν, and

$$\frac{dB(T)}{dT} = \int_0^\infty \frac{dB_\nu(T)}{dT} d\nu. \quad (14)$$

For the computation of $\tilde{\epsilon}_f^W(u,T)$, k_ν^W is assumed to be zero for the range of the wave number overlapped by the 15 μ band of CO_2. Since ϵ_f^W is highly dependent upon temperature below 200K and the atmospheric temperature is mostly above this value, the following identity is used to simplify the numerical computation.

$$\pi B_\infty \cdot \epsilon_f^W(y_\infty^W, T_\infty) = \pi B_C \cdot \epsilon_f^W(y_\infty^W, T_C) + \int_{B_C}^{B_\infty} \tilde{\epsilon}_f^W(y_\infty^W, T)\pi dB, \quad (15)$$

where $B_C = B(T_C)$ and T_C is chosen to be 220K.

$$\mathcal{E}_f^G(u,T) = \left[\int_{\nu_1^G}^{\nu_2^G} B_\nu(T)\{1-\tau_f(k_\nu^G \cdot u)\}d\nu\right] \Big/ \int_{\nu_1^G}^{\nu_2^G} B_\nu(T)d\nu \quad (16a)$$

$$\tilde{\mathcal{E}}_f^G(u,T) = \left[\int_{\nu_1^G}^{\nu_2^G} \frac{dB_\nu(T)}{dT}\{1-\tau_f(k_\nu^G \cdot u)\}d\nu\right] \Big/ \int_{\nu_1^G}^{\nu_2^G} \frac{dB_\nu(T)}{dT} d\nu \quad (16b)$$

and

$$a_f^G(u) = \left[\int_{\nu_1^G}^{\nu_2^G} \{1-\tau_f(k_\nu^G \cdot u)\}d\nu\right] \Big/ (\nu_2^G - \nu_1^G) \approx \mathcal{E}_f^G(u,T) \approx \tilde{\mathcal{E}}_f^G(u,T), \quad (17)$$

where G stands for either the 15 μ band of CO_2 overlapped by the part of the rotation band of water vapor or 9.6 μ band of O_3. The effect of overlapping between the CO_2 band and the water vapor band is taken into consideration by adopting the following approximate equation.

$$\mathcal{E}_f^{C(W)} \approx \tilde{\mathcal{E}}_f^{C(W)} \approx a_f^{C(W)} = a_f^C + a_f^{WVC} - a_f^C \cdot a_f^{WVC}, \quad (18)$$

where a_f^{WVC} is defined by equation (17) for the part of the water vapor band overlapped by the 15 μ band of CO_2 (550–800 cm^{-1}). Strictly speaking, a_f^G depends upon temperature because k_ν^G depends upon temperature. This effect is crudely incorporated for CO_2 by defining the effective mean temperature of the layer concerned [refer to equation (19)]. It was possible to separate the temperature change caused by atmospheric radiation into three parts, i.e., the temperature change due to the 15 μ band of CO_2 including the overlapping with part of the rotation band of water vapor, that due to the 9.6 μ band of O_3, and that due to water vapor. This separation was useful in discussing the role of each absorber. The contribution of the part of the window region of the water vapor spectrum which overlapped with the 9.6 μ band of O_3 was regarded as a contribution of water vapor.

After publication of the previous paper (A), an improvement was made in the infrared absorptivities adopted for our computation. We shall describe them briefly here.

The mean slab transmissivities and emissivities of water vapor for varying amounts of absorber, various temperatures, and various pressures are computed by using the results of experiments and theoretical computations. The general transmission function is obtained from experiments by Howard, Burch and Williams (1955), which could be approximated quite accurately by Goody's random model. This transmission function happens to coincide very well with the plotting of the values of the average transmission given by Palmer (1960) in Fig. 11 of his paper and explains well the pressure dependence of these transmission values. The general absorption coefficient of the rotation band is obtained from Yamamoto's results (1952) and that of the 6.3 μ band is obtained by using the results of the experiment conducted by Howard *et al.* (1955).

The computation of the mean slab absorptivities ε_f^W [equation (13)] of water vapor is carried out for temperatures much lower than 200K. Though the effect of the dependence of k_ν^W on the temperature is neglected for these low temperatures, the temperature shift of Planck's curve for the blackbody radiation is included. This enables us to discuss the thermal equilibrium of high latitudes. The mean slab absorptivities thus computed for various pressures and temperatures are shown in Fig. A-1.

The mean slab absorptivities of the 15 μ band of CO_2, shown in Fig. A-3, are obtained for various pressures by use of experiments performed by Burch *et al.*, (1962). The effect of temperature on the line intensities is taken into consideration, for the range of temperature higher than 218K, using the theoretical estimate of the temperature effect by Sasamori (1959). The effective temperature $\bar{T}$ used for this computation is assumed to be

$$\bar{T} = \left(\int T du_r\right) \Big/ \left(\int du_r\right), \quad (19)$$

where u_r is the effective optical thickness defined by (20).

The absorptivities of the 9.6 μ band of O_3 under different pressures are obtained from an experiment conducted by Walshaw (1957). The temperature dependence of the absorptivity of this band is neglected.

For the numerical computations, the dependence of the absorptivities upon pressure is parameterized by using the effective optical thickness, u_r, defined by

$$u_r = \int (p/p_0)^k \cdot du, \tag{20}$$

where p is pressure, p_0 is the standard atmospheric pressure, u is the amount of absorber, and k is the pressure scaling factor. This factor should be chosen for each absorptivity such that the absorptivity could be expressed as a function of u_r instead of both u and p. It is not possible, however, to express the absorptivity curve as a function of u_r alone for the range of pressure and the amount of absorber covered by the figures in Appendix 1. In order to overcome this difficulty we restricted ourselves to the (p,u) range which was actually encountered in the computation of the thermal equilibrium of the atmosphere. (For example, the combination of a large amount of water vapor and very low pressure or the combination of a small amount of water vapor and high pressure was rarely encountered.) This restriction enables us to represent the pressure dependence of the absorptivity curve by one parameter and to construct a universal curve suitable for our computation.[3] Needless to say, it is desirable to use a two-parameter representation of u and p, but a one-parameter representation is used so as to simplify the numerical computation.

b. Absorption of solar radiation. The scheme for the computation of solar radiation is nearly the same as that described in (A). It is generalized, however, to include the effect of clouds. The absorptivities of solar radiation for water vapor and CO_2 are also improved by use of the more recent experiments conducted by Burch *et al.*, (1962).

The intensity of incoming solar radiation outside the atmosphere is assumed to be 2.00 ly min^{-1} as Johnson (1954) suggested. The albedo of various types of clouds was determined from the statistical study of Haurwitz (1948). The absorptivity of cloud droplets is taken into account by subjectively referring to the theoretical computations performed by Korb, Michalowsky, and Möller (1956). Table 1 gives the albedo of clouds and the absorptivities of cloud droplets adopted for the computations. The reason why these absorptivities are generally smaller than those obtained by Korb *et al.* (1956) is that we excluded here the absorption due to water vapor. The contribution of water vapor to the solar absorption is evaluated separately.

The basic assumptions used for the computation of solar absorption in an atmosphere with clouds are:

1) Solar radiation becomes completely diffused after entering a cloud or after it is reflected by a cloud.
2) All the reflection of insolation by a cloud takes place at the upper surface of the cloud.
3) The effective optical thickness for diffuse radiation is assumed to be 1.66 times larger than that for direct solar radiation.

TABLE 1. Albedos and absorptivities of cloud droplets.

	Albedo	Absorption of cloud droplet
High	0.21	0.005
Middle	0.48	0.02
Low	0.69	0.035

The surface albedo is assumed to be 0.102 except where specified otherwise. For the computation of the local equilibrium of the stratosphere [refer to Section 5b], the latitudinal and seasonal distributions of the surface albedos are calculated by the method suggested by Houghton (1954).

For simplicity, the contribution of Rayleigh scattering to the planetary albedo is assumed to be 7 per cent. According to the results obtained by London (1956), the Rayleigh contribution has about this magnitude and changes little with season. Therefore, this simplification would not cause serious error. The influence of Rayleigh scattering on solar absorption by the atmosphere is neglected.

Fig. 3 illustrates the processes involved in computing the absorption of solar radiation. The total daily mean downward flux of solar radiation at level Z is calculated by the following equations.

$$S_Z = (1-c)\cdot(S_C'-A_Z)\cdot\cos\bar{\zeta}\cdot r + C\cdot\{1-(\alpha+\beta)\}\cdot(S_C'-OA_Z)\cdot\cos\bar{\zeta}\cdot r \tag{21a}$$

$$S_C' = (1-0.07)\cdot S_C, \tag{21b}$$

where S_C is the solar constant and S_C' is the effective solar constant obtained by excluding the part depleted by Rayleigh scattering. α and β are the cloud reflectivity and the absorptivity of cloud droplets, respectively, and C is the cloud amount. $\bar{\zeta}$ is the effective mean zenith angle of the sun defined by the following equation,

$$\cos\bar{\zeta} = \left(\int \cos\zeta(t)dt\right) \Big/ \left(\int dt\right), \tag{22a}$$

in which the integrations are carried out only for hours of daylight. r is defined as

$$r = (\text{total daylight hours})/(24 \text{ hours}). \tag{22b}$$

[3] In the Appendix it will be shown that the results of the thermal equilibrium calculation obtained by this scaling approximation differ a little from those obtained by adopting the effective pressure proposed by Curtis (1952).

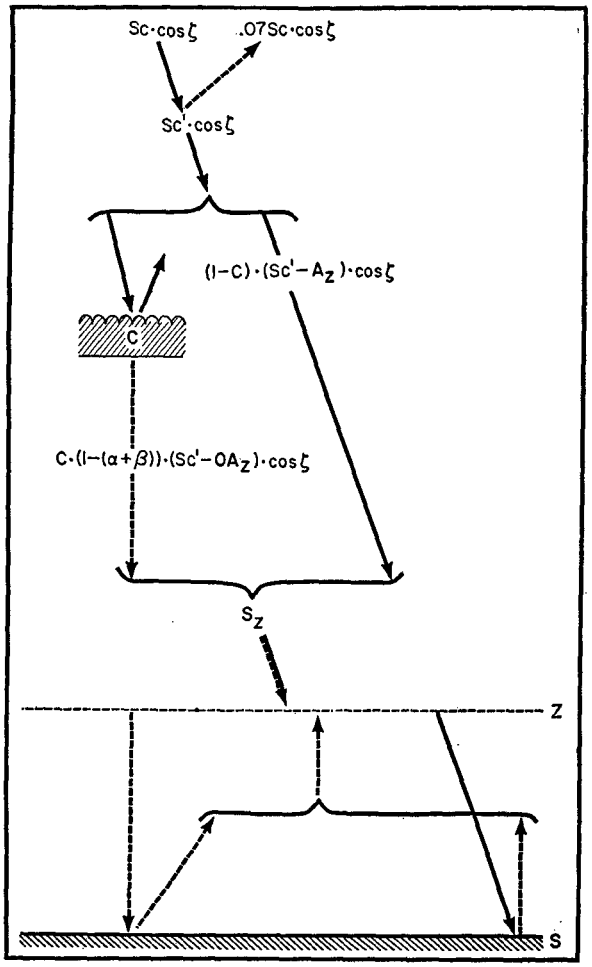

FIG. 3. Vertical distribution of the flux of solar radiation in an atmosphere with clouds.

This approximation of effective mean zenith angle is adopted throughout the present study except where specified otherwise. The results obtained by use of this approximation differ little from those obtained by detailed treatment of the diurnal cycle.

A_Z and OA_Z are the gaseous absorption of solar radiation from the top of the atmosphere to level Z by a clear atmosphere and by an overcast atmosphere, respectively. H_T is the cloud top height. These quantities can be expressed by

$$A_Z = A_Z{}^W + A_Z{}^C + A_Z{}^o \tag{23}$$

$$OA_Z = OA_Z{}^W + OA_Z{}^C + OA_Z{}^o, \tag{24}$$

where

$$A_Z{}^G = a_s{}^G(x^G(\infty, Z)\cdot\sec\tilde{\zeta}) \tag{25}$$

$$OA_Z{}^G = a_s{}^G(x^G(\infty, Z)\cdot\sec\tilde{\zeta} + 1.66x^G(H_T,Z)) \tag{26}$$

and

$$\begin{aligned} x^G(\infty,Z) &= |u_r{}^G(\infty) - u_r{}^G(Z)| \\ x^G(H_T,Z) &= |u_r{}^G(H_T) - u_r{}^G(Z)| \end{aligned} \tag{27}$$

and $a_s{}^G$ is the absorption of solar radiation due to gas G. $u_r{}^G(Z)$, for example, is the effective optical thickness for solar absorption between the earth's surface and level Z.

The total upward reflected radiation at level Z is computed as the sum of radiation reflected by clouds and that reflected by the earth's surface. The effect of the depletion of reflected radiation by clouds is neglected. The total absorption of solar radiation was computed by adding the absorption of downward solar radiation and that of reflected radiation.

The absorption curves of solar radiation for water vapor, computed for various pressures, are shown in Fig. A-4. We used absorptivities for several bands as computed by Yamamoto (1962) [based on an experiment by Howard *et al.* (1955), and taking into consideration the effect of proper self-broadening of water vapor]. The absorption bands included in our computations are 0.72 μ, 0.8 μ, 0.94 μ, 1.1 μ, 1.38 μ, 1.87 μ, 2.7 μ, 3.2 μ, and 6.3 μ. A more recent and refined experiment by Burch *et al.* (1962) coincides very well with the results of the older experiments adopted here.

The absorption curves of solar radiation for CO_2, computed for a range of pressures, are shown in Fig. A-5. An experiment of Howard *et al.* (1955) was used to determine the contribution of the absorption due to the 1.6 μ and the 2.0 μ bands, and an experiment of Burch *et al.* (1962) is used to determine the contribution of the absorption by the 2.7 μ, and the 4.3 μ bands.

In order to compute the absorptivity of solar radiation by O_3, the results of experiments by Vigroux (3000–3700 A) (1953) and those of Inn and Tanaka (2000–3000 A, 4400–7600 A) (1956), were used. The extraterrestrial solar spectrum compiled by Johnson was available for this computation. The result is shown in Fig. A-6.

c. Vertical co-ordinate levels. Eighteen atmospheric levels were used in the present computations. As in our previous computations, the location of the levels is based on a suggestion by Dr. J. Smagorinsky. Let the quantity σ be defined as the following function of pressure:

$$Q \equiv p/p_* = \sigma^2(3-2\sigma), \tag{28}$$

where p_* is the pressure at the earth's surface. If we divide the atmosphere into equal σ-intervals, the pressure-thickness of the layers is thin both near the earth's surface and the top of the atmosphere. Table 2 shows the σ-levels adopted. The temperatures in the radiation formulae given earlier are specified at each level.

d. Distributions of the atmospheric absorbers. Here we shall describe the vertical, latitudinal, and seasonal distributions of gaseous absorbers and clouds which are used.

TABLE 2. Illustration of σ-co-ordinate system. ΔQ is the Q-thickness of each layer.

Level	σ	Q	ΔQ	Approximate height (km)
1	0.02778	0.00227	0.00892	42.88
2	0.08333	0.01968	0.02538	26.38
3	0.13889	0.05251	0.03978	20.08
4	0.19444	0.09872	0.05213	16.08
5	0.25000	0.15625	0.06241	13.28
6	0.30556	0.22304	0.07064	10.98
7	0.36111	0.29702	0.07682	9.03
8	0.41667	0.37616	0.08093	7.48
9	0.47222	0.45838	0.08299	6.08
10	0.52778	0.54162	0.08299	4.88
11	0.58333	0.62384	0.08093	3.73
12	0.63889	0.70297	0.07682	2.86
13	0.69444	0.77696	0.07064	2.06
14	0.75000	0.84375	0.06241	1.40
15	0.80556	0.90128	0.05213	0.86
16	0.86111	0.94749	0.03978	0.46
17	0.91667	0.98032	0.02538	0.18
18	0.97222	0.99772	0.00892	0.02

The distribution of water vapor in the lower troposphere is obtained from the compilation of radiosonde data by London (1956). In order to determine the distribution of water vapor in the upper troposphere, the measurements by Murgatroyd, Goldsmith and Hollings, (1955) and by Murgatroyd (1960) are used. In the stratosphere the frost point of water vapor was assumed to approach 190K. Above the 9-mb level, the assumption of a constant mixing ratio was adopted. For stratospheric water vapor there is a wide range of measured values. The distributions adopted here are consistent with the near-infrared measurement by Houghton and Seely (1960) and are close to the measurement by Mastenbrook at Hyderabad, India (1962). Fig. 5a shows some of the examples of the vertical distribution of water vapor. [Refer to paper (A) for a more detailed explanation.] In view of the uncertainty involved in the measurement of stratospheric water vapor, computations of thermal equilibrium were also performed for a wide range of stratospheric water vapor as shown on the left-hand side of Fig. 9.

The mixing ratio of CO_2 is assumed to be constant throughout the atmosphere (0.0456 per cent by weight).

The seasonal and latitudinal distribution of the total amount of O_3 is given by Normand (1953), while information on the vertical distribution was obtained from Ramanathan and Kulkarni (1960). They constructed charts which showed the latitudinal variation of the vertical distribution of ozone both for the case of a large total amount and the case of a small total amount of ozone. In order to obtain the vertical distribution of ozone at various latitudes which have a different total amount, interpolation is used. Fig. 5b shows examples of vertical distributions of ozone which are obtained by this method.

The various cloud types adopted by London (1956) can be classified into three categories, i.e., high, middle, and low, and the effective heights of cloud tops and cloud bases for these three groups are then defined by taking the weighted means with respect to the amount of each type of cloud. The amounts of these three groups are obtained by summing up the cloud amounts compiled by London.

4. Atmospheric absorbers and thermal equilibrium

a. Thermal equilibrium with average insolation. Before discussing the influence of the various absorbers on the thermal equilibrium of the atmosphere, it is necessary to know how the convective adjustment alters some of the unrealistic features of a pure radiative equilibrium of the atmosphere, such as the cold upper troposphere and the very warm earth's surface described in the introduction. We therefore computed the pure radiative equilibrium and two states of thermal equilibrium with a critical convective lapse rate of 6.5 deg km^{-1} and one with 10.0 deg km^{-1} (dry adiabatic) (Fig. 4). The vertical distributions of gaseous absorbers used in this computation are those for 35N in April (refer to Figs. 5a and 5b). Cloudiness is assumed to be zero and the insolation is assumed to be the annual mean value for the hemisphere (solar constant = 2 ly min^{-1}, $\cos\bar{\zeta}=0.5$, and $r=0.5$). A surface albedo of 0.102 is used. According to Fig. 4, the temperature of the earth's surface in thermal equilibrium with a 6.5 deg km^{-1} adjustment is 300.3K, much more realistic than that of pure radiative equilibrium (332.3K). Also, the temperature of the upper troposphere in thermal equilibrium is warmer and more realistic than that in pure radiative equilibrium. The net incoming solar radiation at the top of the atmosphere is approximately 0.4287 ly min^{-1} for both cases and is compensated by the net outgoing wave radiation at the top of the atmosphere. The net loss of energy from the atmosphere due to long wave radiation is 0.0927 ly min^{-1}. for the case of pure radiative equilibrium, and is 0.2802 ly min^{-1} for the case of thermal equilibrium. In the former case long wave emission from the ground to space plays an important role, whereas in the latter case long wave emission from the atmosphere to space, which must be partly compensated by the convective heat transfer from the ground, becomes important, The isothermal layer and inversion in the lower and upper parts of the stratosphere, correspond very well to observed features of the stratosphere. These results show that the atmosphere in thermal equilibrium does not have some of the unrealistic features of the atmosphere in pure radiative equilibrium.

Having studied the effect of convective adjustment on the radiative equilibrium of the atmosphere, we are now ready to investigate the role of various absorbers in maintaining the thermal structure of the atmosphere. One effective way to do this is to compute the pure radiative equilibrium with and without the absorber. Fig. 6a shows the vertical temperature distributions of

atmospheres containing (H_2O), (CO_2), (H_2O+CO_2), and ($H_2O+CO_2+O_3$)[4] in pure radiative equilibrium. For temperatures below 150K, the accuracy of the computation is poor because of the crude method of incorporating the dependence of transmissivity upon temperature [Section 3a]. The general features of these results, however, would not be altered significantly by improving the accuracy of computation for this low temperature range. According to Fig. 6a, the stratospheric temperature of the (H_2O) atmosphere is significantly cooler than that obtained by Emden (1913). This difference is partly due to the gray body assumption adopted by Emden and may be partly due to the difference in the stratospheric water vapor adopted for the computations. The large difference between the stratospheric temperature of either the (H_2O) or the (H_2O+CO_2) atmosphere, and that of the ($H_2O+CO_2+O_3$) atmosphere shows the importance of ozone in maintaining the stratospheric temperature. In order to analyze this result further, the vertical distribution of various heat balance components for the ($H_2O+CO_2+O_3$) atmosphere in pure radiative equilibrium is shown in Fig. 6b. This figure shows how the absorption of solar ultraviolet radiation by ozone and that of the 9.6 μ band of O_3 help in maintaining the warm stratospheric temperature of the ($H_2O+CO_2+O_3$) atmosphere shown in Fig. 6a. Later, we shall discuss this figure in more detail by comparing it with the vertical distribution of the heat balance components of the atmosphere in thermal equilibrium.

Fig. 6c shows the thermal equilibrium of (H_2O), (H_2O+CO_2) and ($H_2O+CO_2+O_3$) atmospheres. These results also demonstrate the importance of ozone in maintaining the existing temperature of the stratosphere. The height of the tropopause of the atmosphere without ozone is significantly higher than that with

[4] For example, the ($H_2O+CO_2+O_3$) atmosphere means that the atmosphere has a realistic vertical distribution of water vapor, carbon dioxide, and ozone. The effect of clouds was not included.

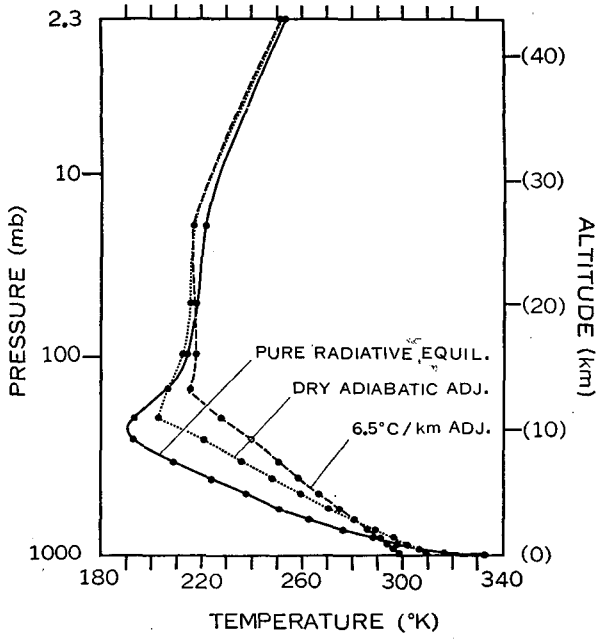

FIG. 4. The dashed, dotted, and solid lines show the thermal equilibrium with a critical lapse rate of 6.5 deg km^{-1}, a dry-adiabatic critical lapse rate (10 deg km^{-1}), and pure radiative equilibrium.

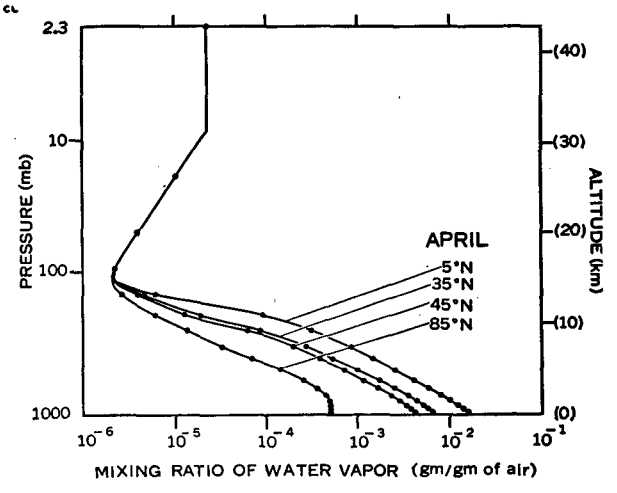

FIG. 5a. Examples of vertical distributions of the mixing ratio of water vapor adopted for our computation.

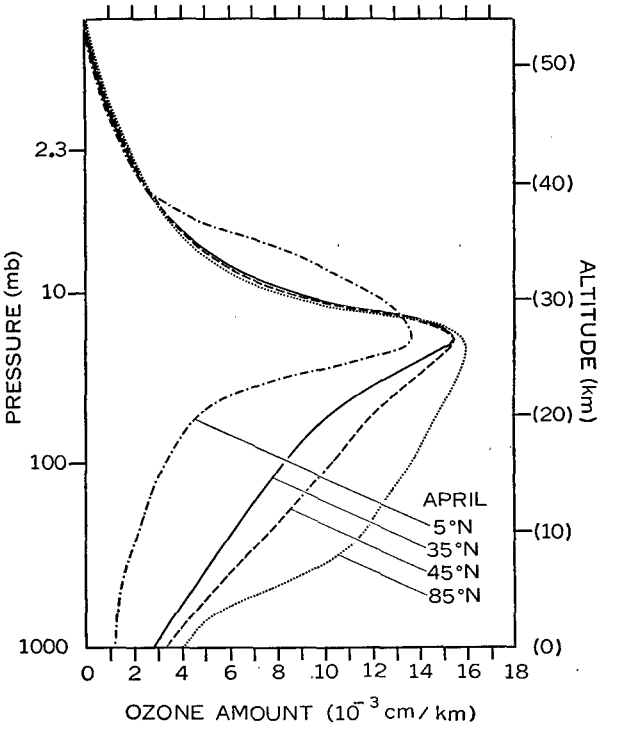

FIG. 5b. Examples of vertical distribution of ozone adopted for our computations.

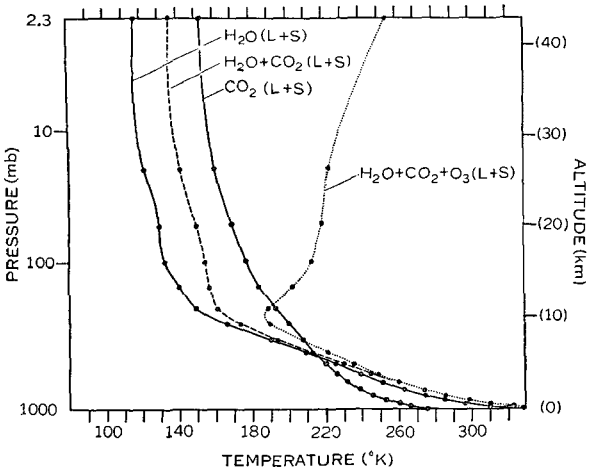

FIG. 6a. Pure radiative equilibrium for various atmospheric absorbers. The distribution of gaseous absorbers at 35N in April are used. $S_c=2$ ly min^{-1}, $\cos\tilde{\zeta}=0.5$, $r=0.5$. No clouds. (L+S) means that the effects of both long wave radiation and solar radiation are included.

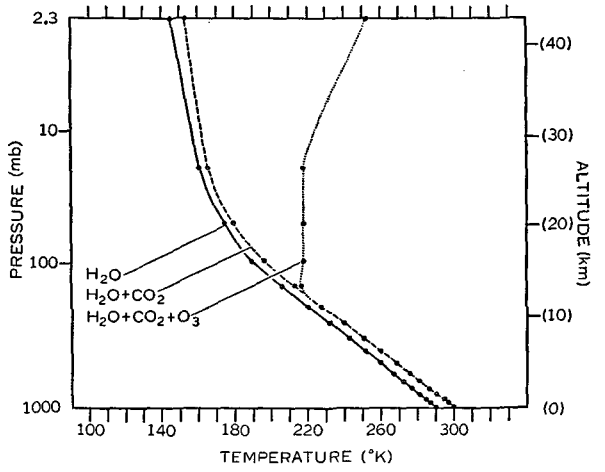

FIG. 6c. Thermal equilibrium of various atmospheres which have a critical lapse rate of 6.5 deg km^{-1}. Vertical distributions of gaseous absorbers at 35N, April, were used. $S_c=2$ ly min^{-1}, $\cos\tilde{\zeta}=0.5$, $r=0.5$, no clouds.

ozone, and the tropopause itself is not marked. Ozone, however, affects the temperature of the earth's surface and troposphere very little (less than 1 deg) judging from the present results. The influence of CO_2 upon the temperature of the earth's surface is about 10 deg. The actual influence would probably be larger than this because the mixing ratio of atmospheric water vapor generally increases as temperature increases and would tend to amplify the effect of CO_2.

b. Thermal equilibrium without insolation. In order to understand the behavior of long wave radiation and to realize the importance of solar heating, the states of pure radiative and thermal equilibrium of the atmosphere were also computed by neglecting solar radiation, substituting therefore a constant surface temperatutre

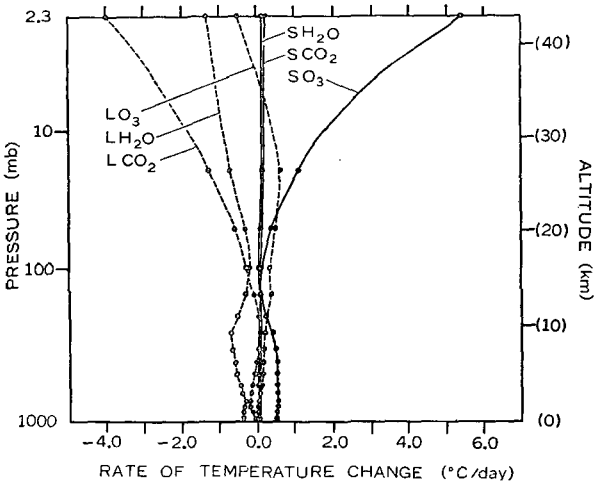

FIG. 6b. Vertical distributions of the rate of temperature change of the ($H_2O+CO_2+O_3$) atmosphere in pure radiative equilibrium due to various absorbers. LH_2O, LCO_2, and LO_3 show the rate of temperature change due to long wave radiation of water vapor, CO_2 (the effect of H_2O overlapping was included), and O_3. SH_2O, SCO_2, and SO_3 show the rate of temperature change due to the absorption of solar radiation by water vapor, CO_2, and O_3.

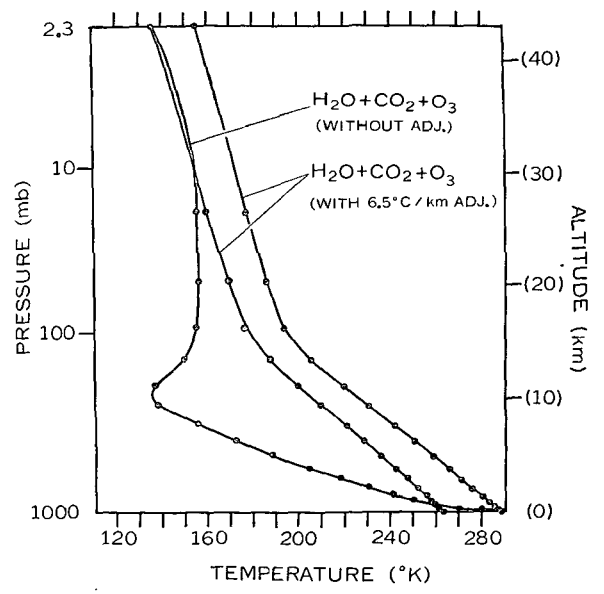

FIG. 6d. Pure radiative and thermal equilibrium without sunshine. The temperature of the earth's surface was fixed at 289K for pure radiative equilibrium, and at 289K or 263K for thermal equilibrium.

as the only heat source. For this series of computations the state of pure radiative equilibrium satisfies the condition of no net flux divergence in the atmosphere but does not satisfy the condition of zero net flux at the top and bottom of the atmosphere. The thermal equilibrium state does satisfy the condition of no net flux divergence in stable layers, but does not satisfy the condition of zero net flux at the top of the atmosphere (refer to Section 2). The critical lapse rate for the convective adjustment is

again assumed to be 6.5 deg km^{-1}. The vertical distributions of gaseous absorbers are shown in Figs. 5a and 5b. Cloudiness is again assumed to be zero. Fig. 6d gives the results for a fixed surface temperature characteristic of the polar region (263K) and for a fixed surface temperature characteristic of middle latitudes (289K). Radiative equilibrium is also shown for the latter temperature. According to this figure, the atmosphere in pure radiative equilibrium has an inversion of temperature at the computed tropopause. Although King (1952) showed that the radiative equilibrium of the atmosphere with a single absorber does not have an inversion, Goody (1947) and Kaplan (1954) suggest that the combined effect of three absorbers could produce the inversion at the tropopause. One of the important effects here is the heating resulting from O_3 absorption of radiation coming from the ground through the water vapor window. This effect is large for a large difference between the temperature of the tropopause and the earth's surface. This inversion, however, disappears when we add the convective adjustment. (Note that the adjustment was made only when the lapse rate exceeded the critical value.) This lack of inversion in the convective curves of Fig. 6d is mainly due to the reduced tropopause—ground difference in temperature and is reminiscent of the vertical distribution of temperature observed during the arctic winter. This result, however, does not mean that the effect of long wave radiation does not play a role in maintaining the isothermal layer or slight inversion just above the tropopause in middle latitudes (Refer to Section 4d and Fig. 8c).

c. Influence of cloudiness. In order to study the influence of clouds on the thermal equilibrium of the atmosphere and the climate of the earth, computations were made of the thermal equilibrium atmosphere with an overcast at various altitudes. The properties of various cloud types for infrared and solar radiation are described earlier in this paper, and the assumed distributions of gaseous absorbers are shown in Fig. 5a and Fig. 5b (April, 35N). The solar insolation is assumed to be the annual mean value for the hemisphere ($Sc=2$ ly min^{-1}, $\cos\bar{\zeta}=0.5$, and $r=0.5$).

The results of these computations are shown in Fig. 7a. On the right hand side of the figure the height of the cloud adopted for each computation is shown. When the height of cirrus is greater than 9 km, the cirrus cloud is heated as a whole. According to our study, the emission from the ground through the atmospheric water vapor window is mainly responsible for this heating. As one might expect, the thinner and the colder the cirrus clouds are, the stronger is this rate of heating. In these computations the heating effect of cirrus is spread out somewhat because of the finite difference scheme. The heating effect of high clouds was first pointed out by

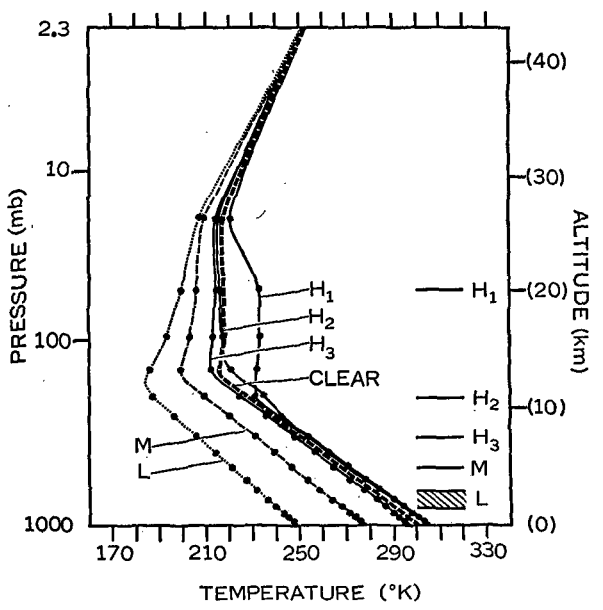

FIG. 7a. Thermal equilibrium of various atmospheres with clouds (the critical lapse rate for convective adjustment is 6.5 deg km^{-1}). On the right hand side of the figure the height of overcast clouds used for each computation is shown, H_1, H_2, and H_3 denoting high clouds, M and L denoting middle and low clouds. As a reference, the equilibrium curve of the clear atmosphere is shown by a thick dashed line.

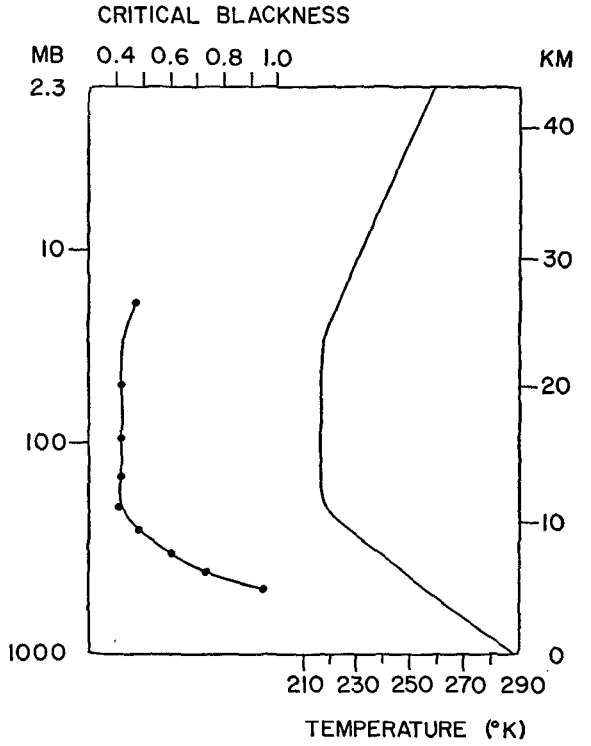

FIG. 7b. On the right hand side of the figure, the vertical distribution of temperature adopted for the computation is shown. On the left hand side, the critical blackness of cirrus for heating the earth's surface is shown. $Sc=2$ ly min^{-1}, $\cos\bar{\zeta}=0.5$, $r=0.5$, no clouds other than cirrus, gaseous absorbers are the distributions at 35N in April.

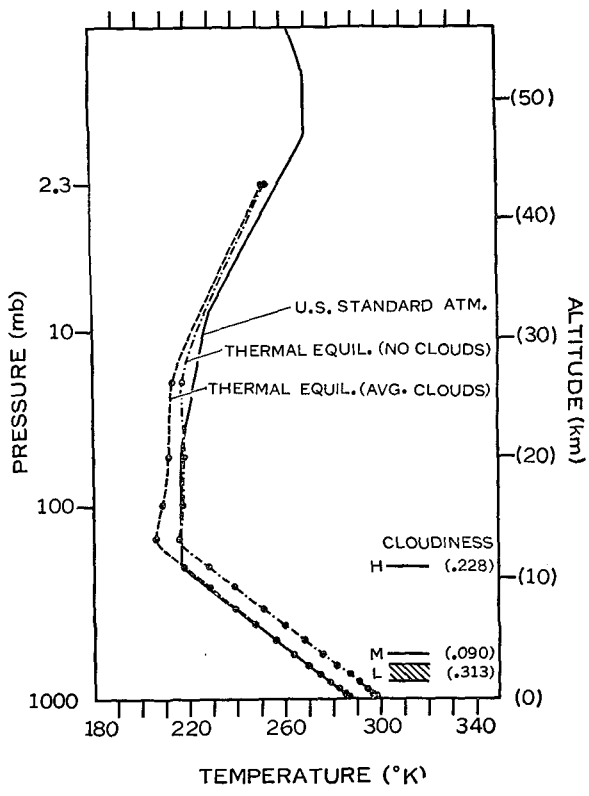

FIG. 8a. Dash-dotted and dashed lines show the thermal equilibrium of the atmosphere with and without cloudiness. The critical lapse rate for convection is 6.5 deg km^{-1}. The cloud amounts and cloud heights are shown on the right hand side. The solid line shows the U. S. Standard Atmosphere.

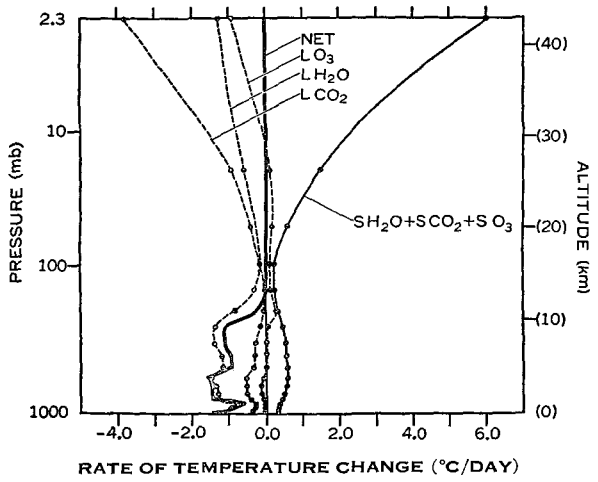

FIG. 8b. Vertical distributions of radiative balance components for the thermal equilibrium of the atmosphere with the average cloudiness shown in Fig. 8a. "Net" means the net rate of temperature change due to all of these components. Refer to Fig. 6b for further explanation.

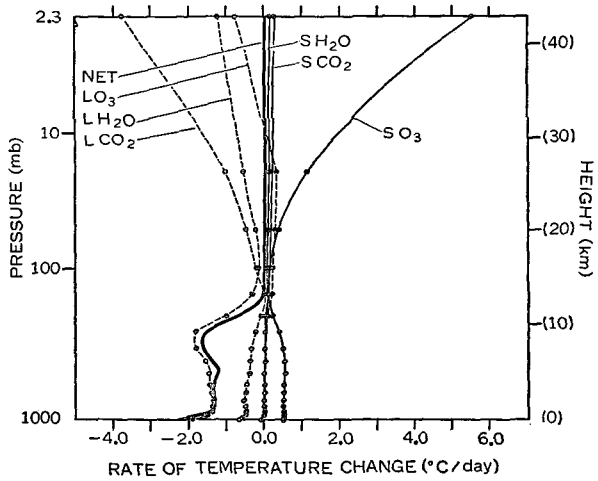

FIG. 8c. Vertical distributions of the radiative heat balance components for the thermal equilibrium of a clear atmosphere. Refer to Fig. 6b for further explanation.

Möller (1948), and might have an important effect on the heat budget of the upper troposphere, as suggested recently by Riehl (1962).

According to Fig. 7a, the influence of cirrus on the temperature of the earth's surface also depends upon the height of the clouds. If the height of cirrus clouds is greater than 9 km and its blackness for infrared radiation is larger than 50 per cent, cirrus has a heating effect on the temperature of the earth's surface. Fig. 7b is included in order to show this effect of cirrus on the climate of the earth's surface in more detail. The distribution of absorbers and solar insolation are the same as those used for the experiments shown in Fig. 7a. The U. S. standard atmosphere was used for these particular computations, and is shown on the right-hand side of the figure. In the left-hand side of this figure, the resulting "critical blackness" of cirrus is shown as a function of altitude; if the blackness of cirrus is larger than this critical value, it has a warming effect on the climate of the earth's surface, and vice versa. According to the figure, the higher the cirrus cloud is in the troposphere, the smaller is the critical blackness. In order finally to determine whether cirrus has a cooling or heating effect on the climate of the earth, a careful measurement of the blackness of cirrus is therefore very important.

As expected, Fig. 7a shows that middle and low clouds have a cooling effect on the temperature of the earth's surface. Since we fix the vertical distribution of the mixing ratio of water vapor, irrespective of temperature, thermal equilibrium of an atmosphere overcast by middle and low clouds (as defined in this study) corresponds to super-saturation. If we prescribed the relative humidity instead of the mixing ratio, the influence of these clouds on the climate of the earth's surface could be greater.

It is interesting to note that the temperature distribution of the upper stratosphere in radiative equilibrium tends to approach a common value irrespective of the cloudiness in the lower atmosphere [Refer to (B) also].

This is probably due to a decrease with increasing altitude of the relative importance of absorption of long wave radiation coming from a low level.

d. Comparison with the standard atmosphere. In order to study the combined effect of the various factors discussed so far, thermal equilibrium was computed (6.5 deg km^{-1} critical lapse rate) including the effect of average cloudiness, as well as all three absorbers. Fig. 8a shows the temperature distribution for thermal equilibrium for both clear and average cloud conditions. The cloud heights and amounts corresponding to average values in middle latitudes are shown in the same figure. The vertical distributions of gaseous absorbers at 35N in April were used (Figs. 5a and 5b) and the insolation was the annual mean for the hemisphere ($Sc=2$ ly min^{-1}, $\cos\bar{\zeta}=0.5$, and $r=0.5$).

With average cloudiness, the computed temperature of the earth's surface is about 286.9K, which is close to the surface temperature of the standard atmosphere. The temperature of the stratosphere turns out to be somewhat lower than the observed temperature for reasons which are difficult to determine. The difference between the computed surface temperature of a clear atmosphere and that of an atmosphere with average cloudiness is about 13 deg. This difference might become larger if we take into consideration the possible change of the mixing ratio of water vapor corresponding to the change of temperature. The computed height of the tropopause is about 13 km, which is about 2 km higher than the tropopause height of the U. S. standard atmosphere. This computed altitude is between the observed height of the polar tropopause and that of the tropical tropopause.

Table 3 lists the magnitude of various heat balance components of these two atmospheres in thermal equilibrium, together with the annual and hemispheric mean heat balance obtained by London (1956). The magnitude of the heat balance components of the atmosphere with average cloudiness in thermal equilibrium compares very well with the annual and hemispheric mean components of heat balance of the actual atmosphere obtained by London. This comparison shows the degree of similarity of our thermal equilibrium atmosphere to the actual atmosphere.

Figs. 8b and 8c show the vertical distributions of various heat balance components for an atmosphere with and without clouds. These results show clearly that the atmosphere in thermal equilibrium satisfies the condition of radiative equilibrium in the stratosphere. In the troposphere, however, a net radiative cooling appears which is equal to the radiative excess of heat at the earth's surface.

According to these figures, the relative importance of the radiative heat balance components varies with altitude. In the troposphere, both long wave radiation and the absorption of solar radiation by water vapor play major roles. In the stratosphere, the relative importance of the absorption of solar radiation by O_3 and that of cooling due to the 15 μ band of CO_2 increase with altitude. Fig. 8b and 8c also suggest that the main cause of the inversion in the upper stratosphere and the isothermal layer in the middle stratosphere is the increase with altitude of the absorption of solar ultraviolet radiation by ozone, and that the warm middle stratosphere helps to maintain the isothermal layer or slight inversion just above the tropopause through the effect of long wave radiation. (Note the sharp decrease of the cooling due to the long wave radiation of water vapor with altitude around the level of tropopause.)

TABLE 3. Integrated heat balance components of thermal equilibrium (ly min^{-1}) of the atmospheres with and without clouds shown in Fig. 8a. Hemispheric annual mean components obtained by London are also shown for comparison.

	Thermal equilibrium		Heat balance
	Clear	Cloudy (average cloudiness)	London
Net outgoing long wave radiation at the top of atmosphere	0.4287	0.3266	0.324
Net incoming solar radiation at the top of atmosphere	0.4286	0.3266	0.324
Atmospheric heating: Long wave	−0.2802	−0.2412	−0.234
Atmospheric heating: Solar radiation	0.0927	0.0901	0.087
Heating of the earth's surface: Long wave	−0.1485	−0.0854	−0.090
Heating of the earth's surface: Solar radiation	0.3360	0.2365	0.237
Eddy transport of energy from the earth's surface to the atmosphere	0.1875	0.1511	0.147

It is interesting to compare the vertical distribution of various heat balances of the atmosphere in thermal equilibrium shown in Fig. 8c with that in pure radiative equilibrium shown in Fig. 6b. The heating due to the 9.6 μ band of the latter is much larger than that of the former owing to the absorption of the emission from the unrealistically warm surface of the earth in pure radiative equilibrium. On the other hand, the net tropospheric cooling in the radiative equilibrium case due to the long wave radiation of water vapor turned out to be smaller than in the thermal equilibrium case; this is a result of the small emission from the cold troposphere and the absorption of the larger emission from the very warm surface temperature of the radiative equilibrium case.

e. Stratospheric water vapor. One of the most uncertain factors involved in the computed thermal equilibrium states is the distribution of water vapor in the stratosphere. As the papers by Gutnik (1962) or Barclay and associates (1960) show, the vertical distribution of stratospheric water vapor is poorly known. It therefore seemed advisable to make computations of thermal

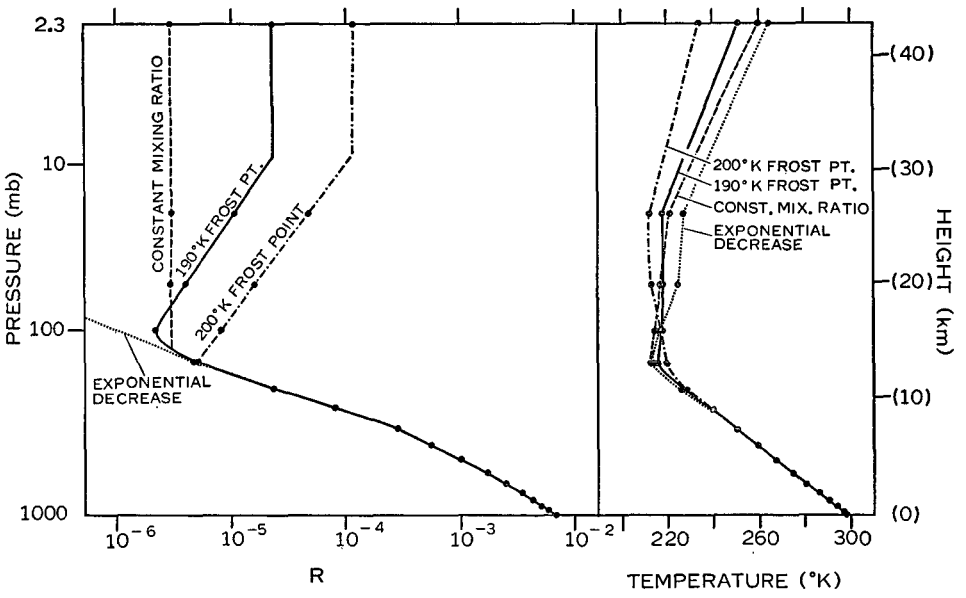

FIG. 9. On the right the thermal equilibrium curves corresponding to various stratospheric water vapor distributions are shown. On the left are the vertical distributions of water vapor. R denotes the mixing ratio of water vapor (gram/gram of air). The critical lapse rate for convective adjustment is 6.5 deg km.$^{-1}$ Distribution of ozone for 35N, April, is used throughout the computation. $S_c=2$ ly min^{-1}, $\cos\bar{\zeta}=0.5$, $r=0.5$. No clouds.

equilibrium with a wide range of stratospheric water vapor, thereby establishing the sensitivity of our results to this factor. The left-hand side of Fig. 9 shows the 4 distributions of water vapor used for this purpose. The constant mixing ratio (3×10^{-6}) case corresponds to the recent measurement by Mastenbrook (1963), who took extreme care to eliminate any contamination by evaporation from his balloon. The 200K frost point compares fairly well with the trial distribution presented by Gutnik (1962). Above the 9-mb level, the mixing ratio was assumed to be constant. The right side of Fig. 9 shows the thermal equilibrium of the atmosphere which corresponds to these distributions of water vapor (other factors were $\cos\bar{\zeta}=0.5$, $Sc=2$ ly min^{-1}, $r=0.5$, no clouds, and ozone at 35N in April).

The upper stratospheric equilibrium temperature depends very much on the distribution of water vapor.[5] As was shown in the previous paper (A), increases of upper stratospheric water vapor lower the temperature of the upper stratosphere. On the other hand, the temperature of the lower stratosphere or of the upper troposphere depends little on the distribution of stratospheric water vapor. This is due to the compensating effect of the convective adjustment, since, as one would expect, this dependence is large for an atmosphere in pure radiative equilibrium [paper (A)]. In spite of quantitative differences between the thermal equilibriums for different distributions of stratospheric water vapor, it may be concluded that the general features of the inversion in the upper stratosphere and of an approximately isothermal lower stratosphere are common to these results. Finally, it should be added that the influence of the stratospheric water vapor on the computed temperature of the earth's surface turned out to be very small.

5. Latitudinal variation of temperature

a. Influence of the latitudinal variation of absorbers. So far we have discussed the role of various atmospheric absorbers in maintaining the observed vertical thermal structure of the atmosphere. Now we consider the dependence of thermal equilibrium upon latitudinal variation of absorbers. Though this problem was investigated in the previous paper (A), it seemed worthwhile to study it again with the convective adjustment.

The influence of latitudinal variation in water vapor and ozone was examined by the series of computations listed in Table 4. Experiments 1, 2, and 3 are useful for evaluating the influence of latitudinal variation in water vapor, and the comparison between experiments 1 and 4 or experiments 3 and 5 is useful for evaluating that of ozone.

Figs. 10a and 10b show the equilibrium temperature with and without the convective adjustment. The difference in tropopause height corresponding to the pole to equator difference of water vapor is about 3 km for pure

[5] Although this dependence of upper stratospheric temperature on the distribution of water vapor is fairly large, it turned out to be significantly smaller in the present work than in the previous work (A), partly because of the difference in mean absorptivities for very small amounts of H_2O and CO_2 under very low pressure.

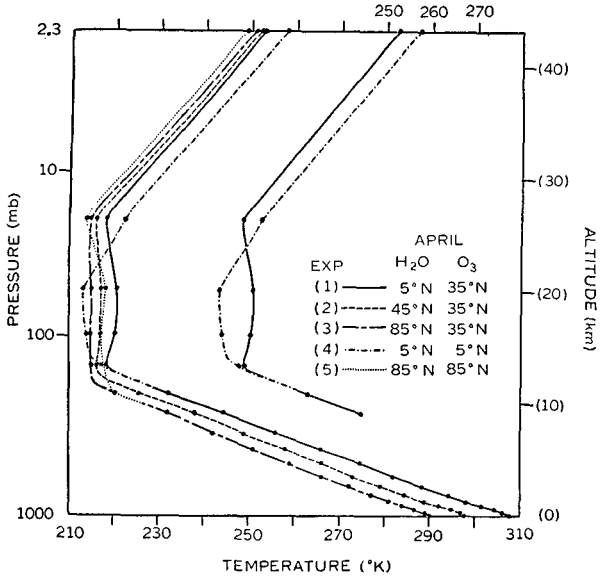

FIG. 10a. Thermal equilibrium of the atmosphere for experiments 1–5. The critical lapse rate for convective adjustment is 6.5 deg km^{-1}.

TABLE 4. Various combinations of the vertical distribution of absorbers. Fig. 5 shows the vertical distribution of absorbers at various latitudes in April. (Sc=2 ly min^{-1}, cosζ=0.5, r=0.5, no clouds.)

Experiment number	H_2O	O_3
1	5N, April	35N, April
2	45N, April	35N, April
3	85N, April	35N, April
4	5N, April	5N, April
5	85N, April	85N, April

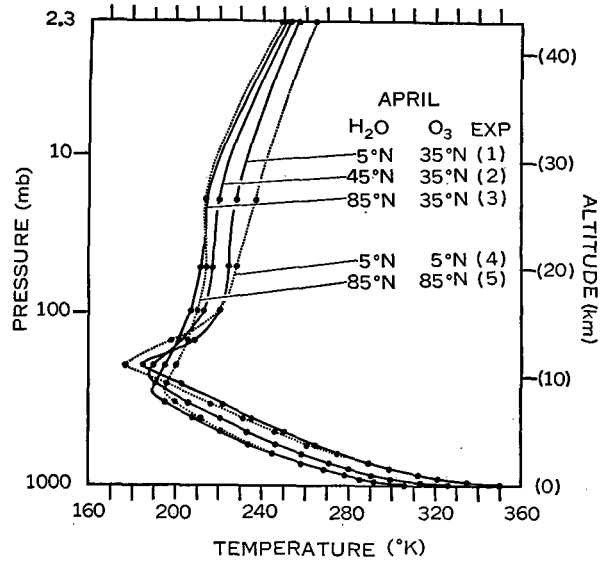

FIG. 10b. The pure radiative equilibrium curves for experiments 1–5.

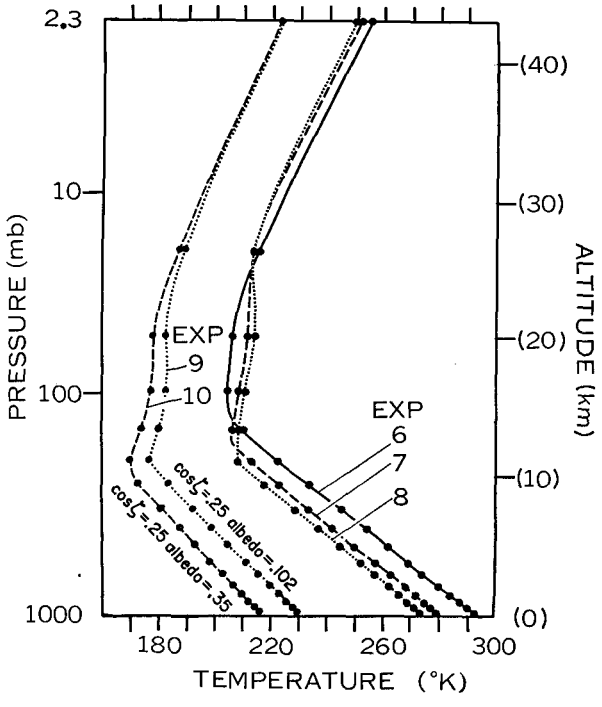

FIG. 11. Thermal equilibrium of the atmosphere for experiments 6–10. The critical lapse rate for convective adjustment is 6.5 deg km^{-1}. Computations are carried out for various distributions of absorbers, sunshine, and albedo. Refer to Table 5.

radiative equilibrium and 2.5 km for thermal equilibrium. The tropopause slope for pure radiative equilibrium is greater because the latitudinal variation of water vapor at the computed tropopause level is larger.

The net effect of latitudinal variation in both gaseous absorbers and clouds, was studied with another series of computations. Table 5 shows the data for this series (Exp. 6–10), and Fig. 11 shows the results. According to this figure, the computed height of the tropopause for the equatorial distribution of absorbers is about 3.5 km higher than that for the polar distribution of absorbers. (Refer to Exp. 6, 7, and 8). The decrease of solar insolation to the polar value (0.25 ly min^{-1}) has very little influence on the height of the tropopause (Refer to Exp. 9). The increase of surface albedo to 0.35 has the effect of lowering the tropopause very slightly (Refer to Exp. 10). These results show that the dependence of tropopause height upon the atmospheric absorbers, surface albedo, and insolation is not large enough to explain quantitatively the observed latitudinal variation of the height of the tropopause. A similar conclusion was obtained in the previous study (A) where the pure radiative equilibrium of the atmosphere with a fixed surface temperature was investigated. It is interesting, however, to note that the tropopause height of the atmosphere in pure radiative equilibrium approximately corresponds to the observed height in higher latitudes where the convective activity is weak, while the tropopause of the

equatorial atmosphere in thermal equilibrium is close to the observed height in lower latitudes where the convective activity is strong. However, it seems certain that the inclusion of large-scale motions (including also the meridional circulation) is needed to explain the latitudinal variation of tropopause height and temperature of the lower stratosphere.

TABLE 5. Distributions of absorbers, mean zenith angle, insolation, and albedo of earth's surface adopted for Exp. 6–10.

Experiment number	Distribution of absorbers and clouds	$\cos\bar{\zeta}$	Insolation ($Sc\times r\times\cos\bar{\zeta}$) (ly min^{-1})	Albedo
6	5N, April	0.5	0.5	0.102
7	45N, April	0.5	0.5	0.102
8	85N, April	0.5	0.5	0.102
9	85N, April	0.25	0.25	0.102
10	85N, April	0.25	0.25	0.35

According to Experiments 1 and 3 of Fig. 10a, (equilibrium with convective adjustment), the computed temperature of the earth's surface for the distribution of equatorial water vapor is about 17 deg higher than that for the polar water vapor distribution. This difference in temperature exists throughout the troposphere but it becomes very small in the stratosphere. This configuration of temperature helps to produce the latitudinal variation of the height of the tropopause. Table 6 shows the consequence of this difference in the surface temperature.

TABLE 6. Heat balance of the earth's surface (ly min^{-1}) for some experiments shown in Fig. 10a. A positive sign means an energy gain for the earth's surface. Refer to Table 4 for identification of the experiments.

Exp.	Net long wave radiation at earth's surface	Net solar radiation at earth's surface	Conductive and diffusive transfer of energy at the interface
1 (H_2O, 5N, April)	−0.1118	0.3223	−0.2105
2 (H_2O, 45N, April)	−0.1650	0.3417	−0.1767
3 (H_2O, 85N, April)	−0.2328	0.3638	−0.1310

According to this table the cooling of the earth's surface due to long wave radiation is much larger for the distribution of water vapor in high latitudes than in low latitudes. On the other hand, the amount of solar radiation differs little with the amount of water vapor. (Note that the same insolation was adopted for experiments 1–5.) Therefore the resultant intensity of convection can be larger for the distribution of water vapor in the equatorial region than that in the polar region. Although it is clear that more abundant solar radiation in low latitudes is the primary reason for active convection in that region, the radiative effect of abundant water vapor is also one of the factors for strengthening convection in low latitudes.

The latitudinal variation of the distribution of ozone also has an interesting effect. If we compare experiments 1 and 4 in Fig. 10a (equilibrium with convective adjustment), the equatorial distribution of ozone tends to make the isothermal part of the stratosphere thinner than does the distribution of ozone in high latitudes. In more detail, the equatorial distribution of ozone tends to create a stronger inversion and a cooler tropopause than does the polar distribution. This tendency is more pronounced for the case of pure radiative equilibrium than for the thermal equilibrium. However, the result of Exp. 6 suggests that this effect of ozone distribution is not strong enough to form the very sharp tropopause actually observed in the tropics. The height of the computed tropopause is about 14 km. It is somewhat lower than the observed height (16 km), partly because of the lack of a sharp tropopause. (Note that the temperature of the earth's surface turned out to be close to that at the equator.) As Fig. 5a shows, the mixing ratio of water vapor adopted for Exp. 6 has a minimum at the level of the equatorial tropopause. This is reasonable in view of the very low temperature at this level. Since water vapor has a cooling effect, one would not expect a sharp minimum of temperature as a result of the radiative balance alone at the place where the mixing ratio of water vapor is a minimum. These results suggest the importance of the large scale dynamical effects such as meridional circulation in maintaining the extremely cold temperature at the equatorial tropopause and raising the top of the convective layer. Fig. 11 also shows that the computed temperature of the lower stratosphere for the distribution of absorbers for 85N, April (Exp. 8) is slightly warmer than for the distribution of absorbers at 5N, April (Exp. 6). As later results demonstrate, this tendency is far too small to explain the observed equator-pole increase of temperature with latitude.

b. Local radiative equilibrium of the stratosphere. So far, we have investigated the influence of the latitudinal variation of absorbers on the thermal equilibrium of the whole atmosphere. Next, we shall discuss the radiative equilibrium of a stratosphere overlying a troposphere whose temperature is very close to the observed value. It is hoped that this study will give us some information on the radiative balance of the stratosphere as well as the role of radiative processes in maintaining the observed temperature of the stratosphere. For this series of computations the temperature of the lower troposphere (541.6 mb down to the earth's surface) was taken as the observed value. In the upper troposphere (above the 541.6-mb level) the critical lapse rate for convective adjustment was set at 7 deg km^{-1}, which is a typical observed lapse rate for this region. The local equilibrium of the stratosphere was then computed for different seasons as an asymptotic state of the initial value problem. The results are shown in Fig. 13, and for comparison, the observed temperature is shown in Fig. 12.

According to these figures, there are various dis-

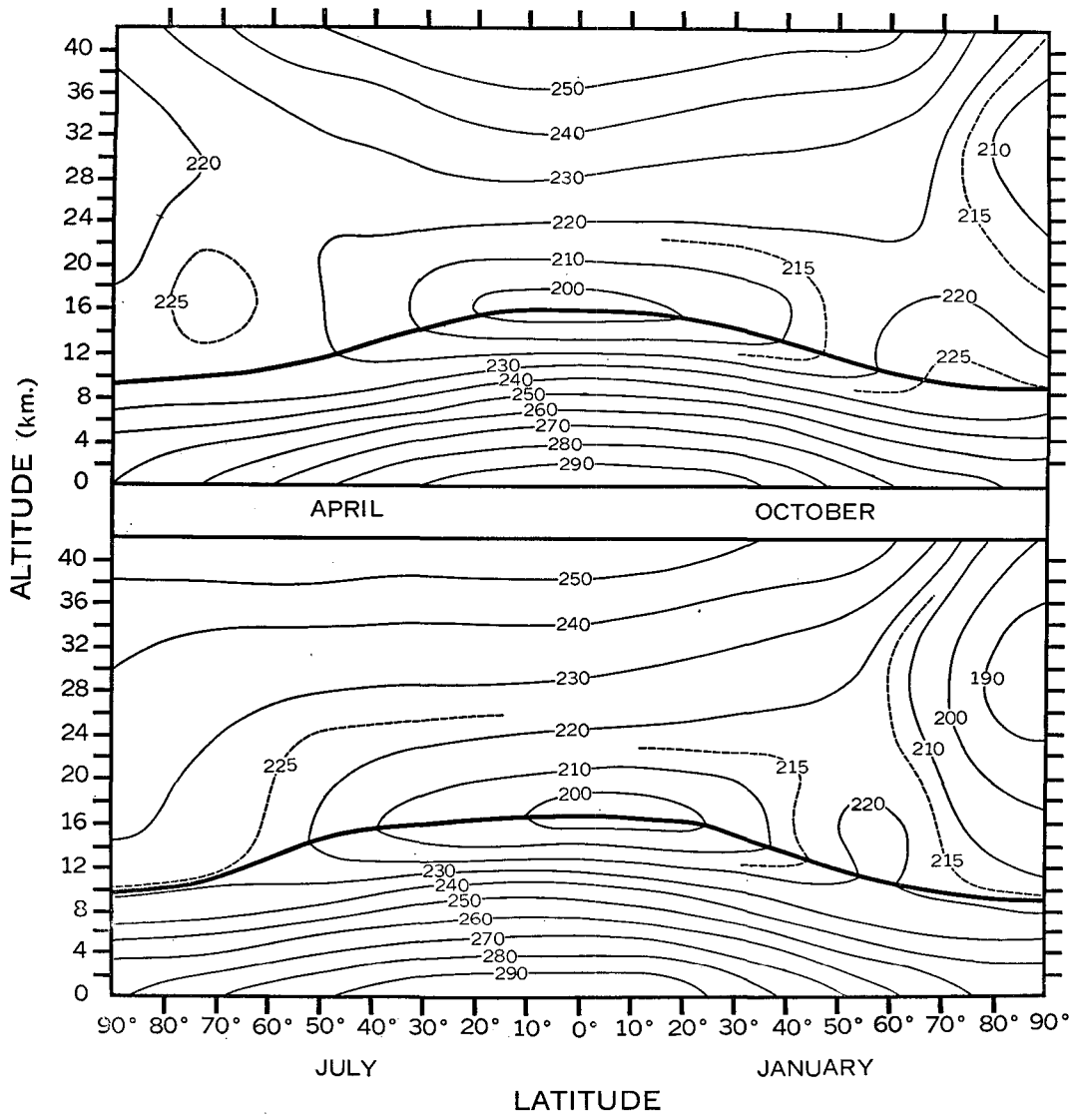

FIG. 12. Distribution of the observed temperature (deg k) in the northern hemisphere for different seasons. From J. London (1956).

crepancies and similarities between the temperature distribution of the actual stratosphere and the computed stratosphere in local radiative equilibrium. For example, the latitudinal variation of the equilibri um temperature of the upper stratosphere in the summer hemisphere was computed to be very small. This featu re corresponds very well with the observed distributio n. On the other hand, the latitudinal decrease of temperature of the upper stratosphere (at 30–40 km) of the winter hemisphere is computed to be much larger than that observed. This suggests a large radiative imbalance in the polar region of the upper stratosphere and a northward transport of heat into this region during the winter. The computed latitude of the maximum temperature gradient in a north-south direction at an altitude of 30–40 km is about 65N and coincides well with the observed latitude of the maximum gradient and the polar night jet stream.

In order to understand this local stratospheric equilibrium better, we have prepared Fig. 14. This figure shows the latitudinal distribution of heating from absorption of solar radiation. It compares well with the results of solar absorption obtained by Murgatroyd and Goody (1958).[6] Since the contribution of solar absorption due to water vapor and carbon dioxide is very small in the stratosphere (Fig. 8b), the latitudinal variation of solar heating in the stratosphere reflects

[6] The distribution of the solar heating shown in Fig. 14 is obtained by numerically integrating the absorption of solar radiation computed every 30 min., and is not the same as the distributions used for obtaining Fig. 13 (Refer to Section 3b). The difference between them, however, is very small.

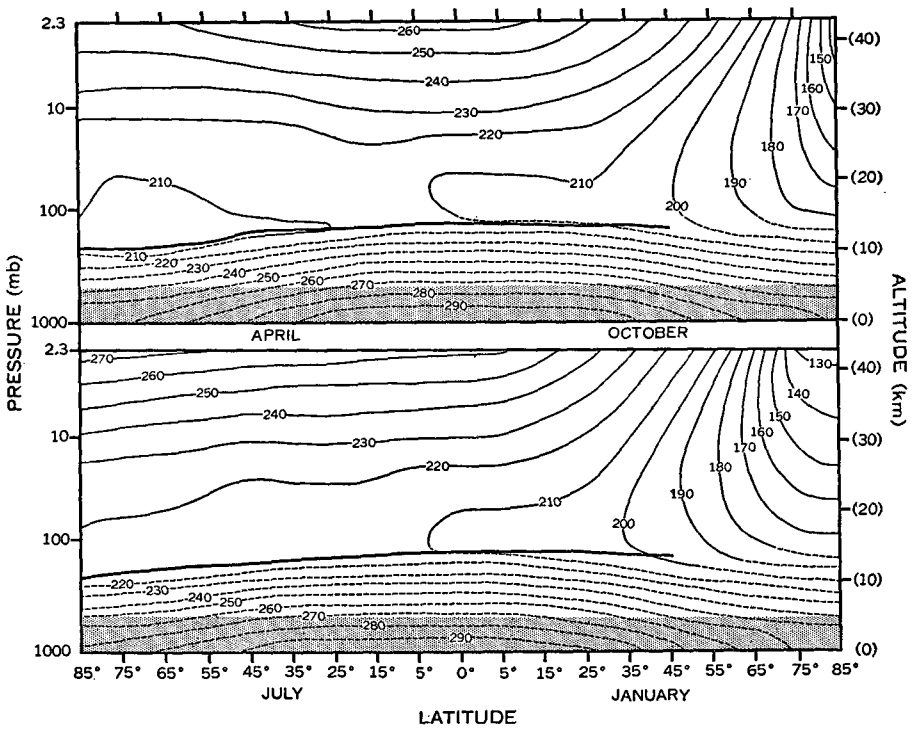

FIG. 13. The local radiative equilibrium temperature of the stratosphere. The shaded area is the region where the temperature was fixed at the observed value. Above the shaded area the state of the convective equilibrium, whose critical lapse rate for convective adjustment is deg km^{-1}, is shown. The region covered by solid lines is in local radiative equilibrium.

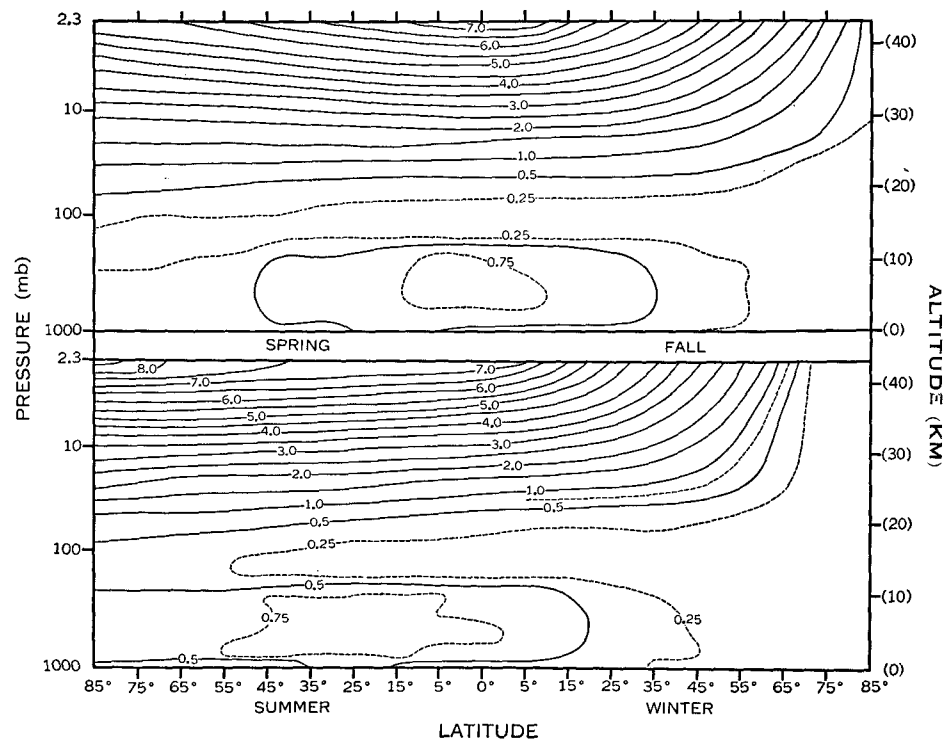

FIG. 14. Vertical distribution of the rate of temperature change (deg day^{-1}) due to absorption of solar radiation.

mainly latitudinal variation of solar radiation and ozone. A comparison among Figs. 12, 13, and 14 shows the solar heating from absorption by ozone is very important in maintaining and explaining the latitudinal distribution of temperature in the upper stratosphere.

One of the most important discrepancies between the observed and the computed temperature distribution (Figs. 12 and 13) is the complete lack of a latitudinal increase of computed temperature of the lower stratosphere in winter and fall, though there is a slight increase in spring and summer. This observed latitudinal increase of temperature is probably due to the combined effect of meridional circulation, vertical transport of heat in large-scale eddys, and horizontal transport of heat against the temperature gradient by large-scale eddys. The last of these was originally emphasized by White (1954). As a result of this discrepancy the latitudinal variation of the tropopause height hardly appears in fall and winter, though some variation appears in the distribution computed for spring. By prescribing the tropospheric temperature to be close to the observed distribution, we have in effect included the hydrodynamic contribution to the maintenance of the latitudinal gradient of the tropospheric temperature, but did not include the accompanying dynamical effect on the latitudinal distribution of stratospheric temperature. This is the reason why we get very little latitudinal variation of the height of the tropopause for winter and fall when the intensity of the northward transport of heat in the lower stratosphere 75–100 mb level) is observed to be as large as it is in the troposphere (Murakami, 1962). Therefore, these results do not contradict the previous result, that the thermal equilibrium of the atmosphere indicates a significant dependence of the height of the tropopause on the latitudinal variation of absorbers, as shown in Fig. 11.

According to Fig. 13, the computed temperature for the polar night keeps decreasing monotonically with increasing altitude, whereas the observed temperature reaches a minimum around 30 km (Fig. 12). One can speculate on the possibility of horizontal advection of heat in large-scale motions at 40 km, where both the computed and observed latitudinal temperature gradient are much larger than for any lower level.

6. Summary and conclusions

1. It is possible to obtain a vertical distribution of the temperature of the atmosphere, which almost exactly satisfies the condition of radiative or thermal equilibrium, as the asymptotic steady state of the initial value problem. The difference between the net outgoing long wave radiation and the net incoming solar radiation at the top of the atmosphere in the experiment is of the order of 5×10^{-4} times either of these two quantities. The maximum rate of temperature change for this final state is 10^{-3} deg day^{-1}. The difference in temperature from the true equilibrium state is about 0.1 deg. It takes about 1 or 2 years to approach this state from an isothermal atmosphere of either 360K or 170K.

2. The atmosphere in pure radiative equilibrium and in thermal equilibrium has the tropopause at approximately 10 km and 13 km, respectively. The temperature of the earth's surface of the former is 332.3K, and that of the latter is 300.3K. For this computation, the annual average insolation was adopted. For the atmosphere in radiative equilibrium, the long wave emission from the ground to space plays an important role, whereas for that in thermal equilibrium, the long wave emission from the atmosphere to space, which must be substantially compensated by the convective heat transport from the ground, becomes important.

3. A comparison among the thermal equilibrium states of an (H_2O) atmosphere, an (H_2O+CO_2) atmosphere and an ($H_2O+CO_2+O_3$) atmosphere, demonstrates the importance of ozone in maintaining the existing distribution of temperature in the stratosphere. The former two cases without ozone have neither a clearcut tropopause nor an inversion in the stratosphere and have a much cooler stratosphere than that observed. The existence of ozone hardly influences the computed temperature of the earth's surface.

4. The pure radiative equilibrium of an atmosphere without solar absorption, but with a fixed temperature at the earth's surface 289K, has an inversion of temperature just above the level of the tropopause, from the combined effect of the infrared radiation of water vapor, CO_2, and O_3. The computed temperature of the stratosphere thus obtained is very low. If we compute the thermal equilibrium for this case by including a convective adjustment (critical lapse rate 6.5 deg km^{-1}), this inversion disappears, and the temperature of the stratosphere decreases monotonically with increasing altitude.

5. If we assume the albedo of cirrus clouds for solar radiation to be 20 per cent and the blackness of cirrus for infrared radiation to be 50 per cent, cirrus existing higher than about 9 km has a heating effect on the earth's surface in thermal equilibrium. Therefore it is rather difficult to determine whether actual cirrus has a heating or cooling effect on the surface climate. Low and middle clouds invariably have a cooling effect on the temperature of the earth's surface.

If the level of clouds or any sort of gray body is higher than 9 km, they tend to be heated instead of cooled by long wave radiation. This heating is due to the difference between the temperature of the clouds and the earth's surface.

6. The thermal equilibrium of an atmosphere with average cloudiness, annual average insolation for the hemisphere, vertical distribution of absorbers typical of 35N in April, and critical lapse rate for convective adjustment of 6.5 deg km^{-1} has a surface temperature of 286.9K, fairly close to the observed value and about

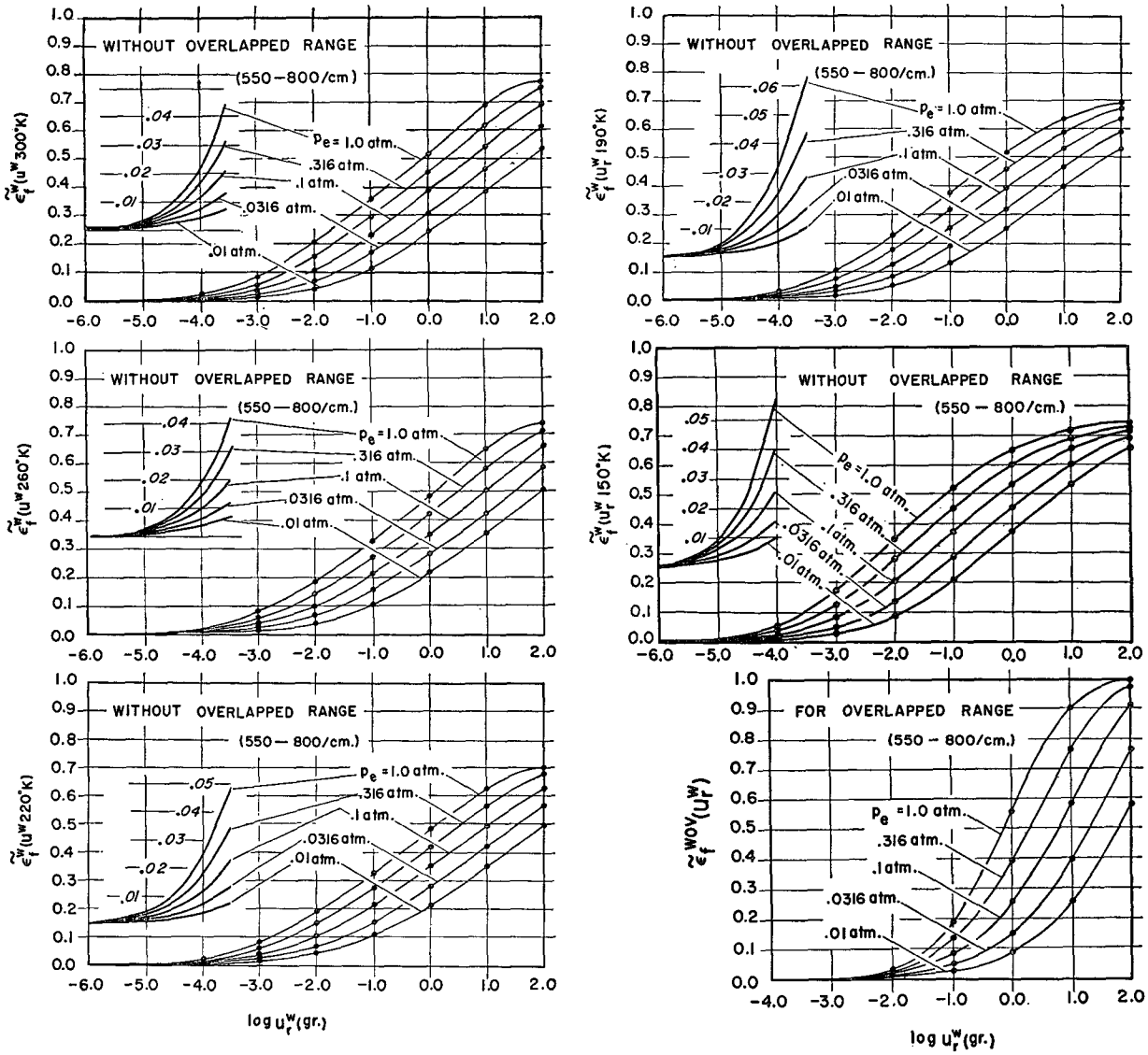

FIG. A-1. The mean slab absorptivities of water vapor for various pressures and temperatures. The mean slab absorptivity of water vapor for the range overlapped with the 15 μ band of CO_2 is shown in the lower right corner. The mean slab absorptivity and the logarithm (base 10) of the effective optical thickness (gram cm^{-2}) are the ordinate and abscissa, respectively.

13 deg colder than the computed temperature of the earth's surface with a clear atmosphere. The height of the tropopause is about 13 km. The energy exchange between the atmosphere and the earth's surface due to the processes other than radiative transfer is 0.151 ly min^{-1}.

7. The net influence of the pole to equator variation of various absorbers on the height of the tropopause in thermal equilibrium is about 3.5 km and is not large enough to explain quantitatively the latitudinal variation of the tropopause.

8. The computed temperature of the earth's surface in thermal equilibrium (critical lapse rate for convective adjustment = 6.5 deg km^{-1}, insolation = annual and hemispheric average, ozone for 35N in April) for an equatorial distribution of water vapor is about 17 deg warmer than that for a polar distribution of water vapor in April. The equatorial distribution of water vapor tends to create a much larger convective exchange of energy between the atmosphere and the earth's surface than does the polar distribution.

9. The equatorial distribution of ozone tends to make the isothermal part of the stratosphere thinner than does the distribution of ozone in higher latitudes. This tendency, however, is not pronounced enough to explain completely the sharpness of the equatorial tropopause.

10. The local radiative equilibrium of a stratosphere lying on a troposphere whose temperature is close to the

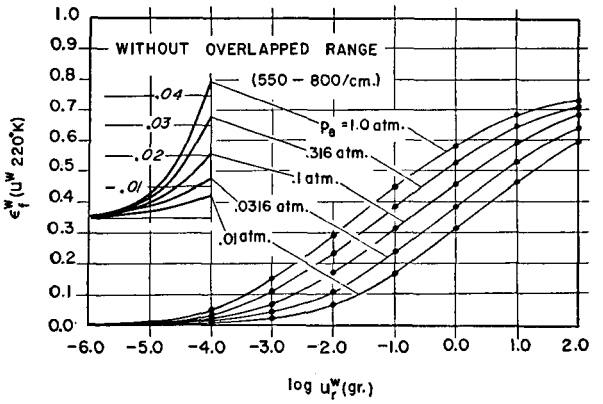

FIG. A-2. The slab emissivity of water vapor for 220K under different pressures. The slab emissivity and the logarithm (base 10) of the effective optical thickness (gram cm^{-2}) are the ordinate and abscissa, respectively.

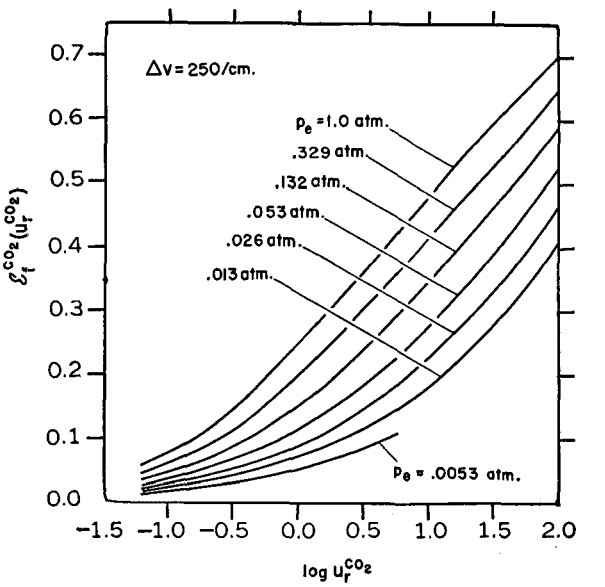

FIG. A-3. The mean slab absorptivity of CO_2 under various pressures. The mean slab absorptivity and the logarithm (base 10) of the effective optical thickness (cm at N.T.P.) are the ordinate and abscissa, respectively.

observed temperature, was computed. In the summer hemisphere the computed temperature of the upper stratosphere depends little upon latitude, in agreement with the observed distribution. In the winter hemisphere a strong latitudinal contrast of the upper stratospheric temperature is computed to be close to the observed latitude of the polar night jet. The equilibrium temperature of the stratosphere at the winter pole, however, is much lower than that observed and suggests a large radiative inbalance in the real atmosphere in this region. The computed temperature of the winter polar stratosphere decreases with increasing altitude (no inversion, no clear-cut tropopause), whereas the observed temperature stops decreasing around the height of 30 km. These results suggest a large northward flux of heat in the upper stratosphere during winter.

The stratospheric radiative equilibrium does not have the observed feature of an increase of temperature with increasing latitude. Although a very slight increase appeared in the local equilibrium for spring and summer, a very steep decrease with increasing latitude appeared in that for winter and fall. The conclusion of this study is that large-scale motions are required to explain this feature.

Acknowledgments. This work constitutes part of an effort to construct an advanced general circulation model which was initiated by Dr. Joseph Smagorinsky. We are grateful to him for his constant encouragement and useful ideas. We are also indebted to Drs. D. K. Lilly, K. Miyakoda and particularly K. Bryan for their very constructive criticism and suggestions.

It is a pleasure to thank Mrs. Lou Ann Sangster whose assistance in computer programming was indispensable. Thanks are due to Mrs. Mary Marini and Mrs. Marylin Varnadore who assisted in computing absorptivity and analysing data, and to Mrs. J. A. Snyder, Mr. G. Reynolds, and Mrs. R. A. Brittain who helped in preparing the manuscript.

APPENDIX

1. Absorptivity

The mean slab absorptivity and slab emissivity of water vapor are shown in Figs. A-1 and A-2, respectively. The mean slab absorptivity of CO_2 is shown in Fig. A-3. A detailed explanation of these figures will be found in Section 3.

The curves of solar absorption for water vapor, CO_2, and O_3 which were constructed for our present study are shown in Figs. A-4, A-5, and A-6.

2. Pressure effect

In this work the effect of pressure on the absorption or emission of a non-homogeneous atmospheric layer is incorporated by use of a so-called "scaling approximation" for simplicity of computation. In order to prevent an error due to this approximation, we use laboratory data at pressures close to those at which computations are made (Refer to the last paragraph of Section 3a for a more detailed explanation). Therefore, it is expected that the pressure effect is incorporated fairly accurately. It seems desirable, however, to repeat the computations of thermal equilibrium, adopting the Curtis approximation, the error of which has been discussed by many authors. For this test, the effective

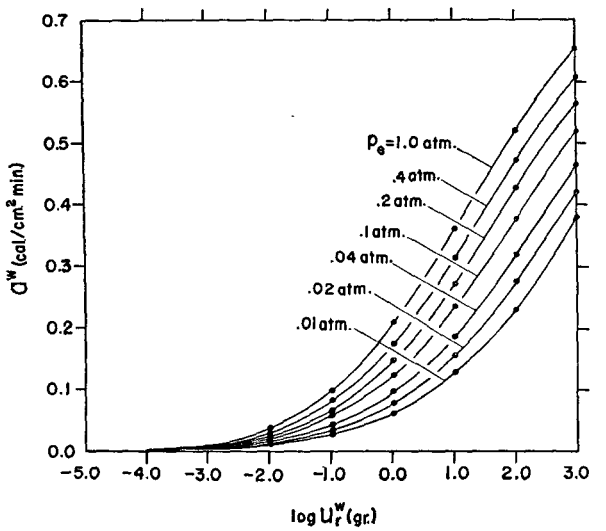

FIG. A-4. Absorption of solar radiation by water vapor under various pressures. The rate of absorption (cal min^{-1} cm^{-2}) and the logarithm (base 10) of the effective optical thickness (gram cm^{-2}) are the ordinate and abscissa, respectively.

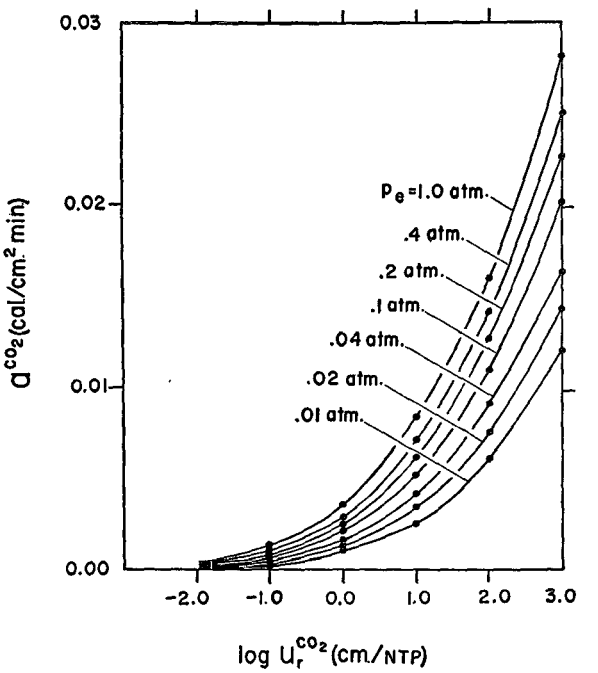

FIG. A-5. Absorption of solar radiation by CO_2 under various pressures. The rate of absorption (cal min^{-1} cm^{-2}) and the logarithm (base 10) of the effective optical thickness (cm at N.T.P.) are the ordinate and abscissa, respectively.

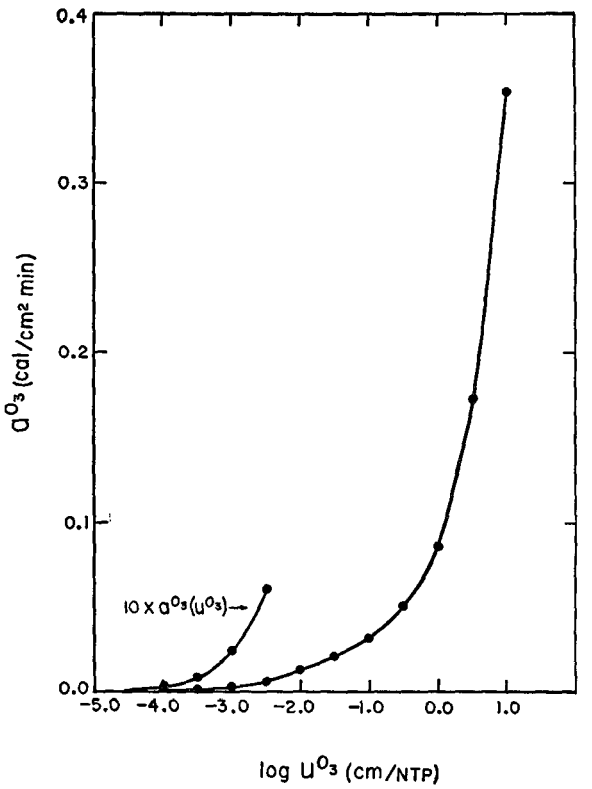

FIG. A-6. Absorption of solar radiation by O_3 under various pressures. The rate of absorption (cal min^{-1} cm^{-2}) and the logarithm (base 10) of the effective optical thickness (cm at N.T.P.) are the ordinate and abscissa, respectively.

pressure $\bar{p}$ of a non-homogeneous layer is defined as

$$\bar{p}=\left(\int P du\right)\Big/\left(\int du\right). \qquad \text{(A-1)}$$

Using this effective pressure, it is possible to compute the rate of temperature change and accordingly to obtain the thermal equilibrium of the atmosphere. In Fig. A-7, the result obtained in this way is shown with that obtained by using the scaling approximation. The difference in equilibrium temperature turns out to be small. As long as we use the laboratory data at pressures close to those at which computations were made, the two different methods of incorporating the effect of pressure do not produce very different results.

3. Temperature change due to the 9.6 micron band of ozone

In order to get some idea of the behavior of our computation scheme of radiative transfer, the rate of temperature change due to the 9.6 μ band of O_3 obtained by Hitchfeld and Houghton (1961) is compared with that obtained by our scheme. On the left hand side of Fig. A-8 are shown the vertical distributions of temperature and O_3 which they adopted. On the right hand side of this figure, the results of our computations for the same distributions of temperature and ozone are given together with their results (dotted lines). The general features of our results are quite similar to theirs.

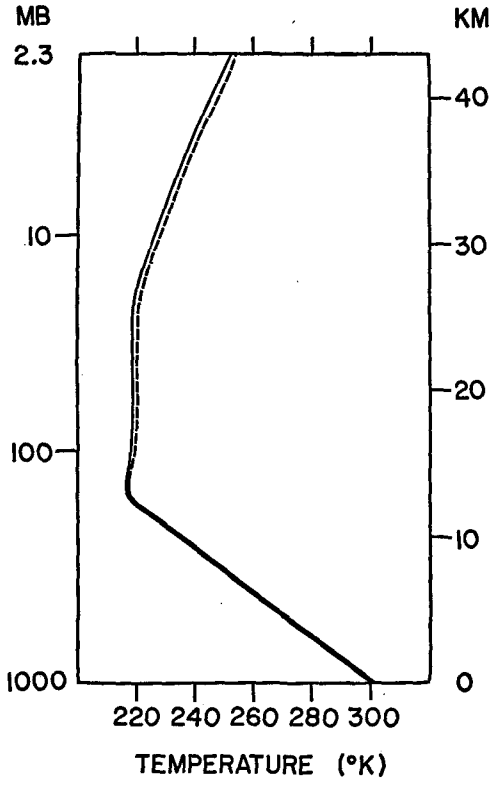

FIG. A-7. Thermal equilibrium obtained by using the scaling approximation (solid line) and by adopting the effective pressure defined by equation (A-1). $S_c = 2$ ly min^{-1}, $\cos\bar{\xi} = 0.5$, $r = 0.5$. No clouds. Gaseous absorbers: distributions of 35N, April.

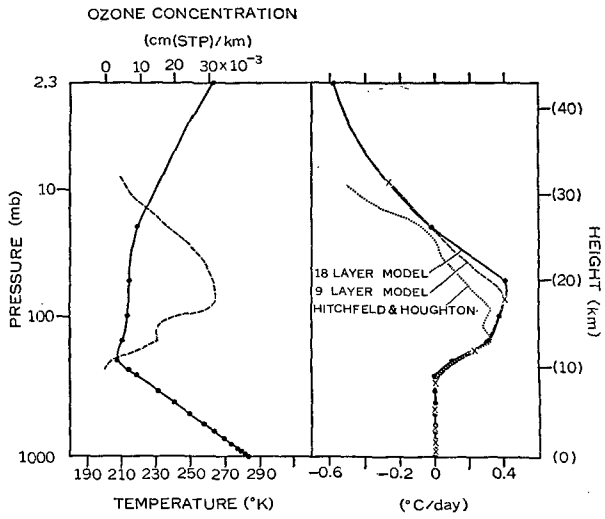

FIG. A-8. On the right, the rate of temperature change obtained by Hitchfeld and Houghton (1961) (dotted line) is shown together with that obtained by our scheme (solid and dashed lines). On the left are shown the vertical distributions of O_3 (dashed line) and temperature (solid line).

REFERENCES

Barclay, F. R., M. J. W. Elliot, P. Goldsmith and J. V. Jellay, 1960: A direct measurement of the humidity in the stratosphere using a cooled-vapor trap. *Quart. J. R. meteor. Soc.*, **86**, 259–264.

Burch, D. E., D. Grayvnak, E. B. Singleton, W. L. France and D. Williams, 1962: Infrared absorption by carbon dioxide, water vapor, and minor atmospheric constituents. Ohio State University, Contract AF 19(604)-2633 AFCRC-62-698, 316 pp. (OTS No. AD-287-406, Xerox $19.75).

Curtis, A. R., 1952: Discussion of Goody's "A statistical model for water vapor absorption." *Quart. J. R. meteor. Soc.*, **78**, 638.

Emden, R., 1913: Über Strahlungsgleichgewicht und atmosphärische Strahlung ein Beiträg zur Theorie der oberen Inversion. *Sitzungsberichte*, Akademie der Wissenschaften, München, No. 1, 55–142.

Goody, R. M., 1949: The thermal equilibrium at the tropopause and the temperature of the lower stratosphere. *Proc. Roy. Soc., A*, **197**, 487–505.

Gowan, E. H., 1928: The effect of ozone on the temperature of the upper atmosphere. *Proc. Roy. Soc., A*, **120**, 655–669.

Gutnick, M., 1962: Mean annual mid-latitude moisture profile to 31 km. *Air Force Surveys in Geophysics*, No. 147, 30 pp.

Haurwitz, B., 1948: Insolation in relation to cloud type. *J. Meteor.*, **5**, 110–113.

Hitchfeld, W., and J. T. Houghton, 1961: Radiative transfer in the lower stratosphere due to the 9.6 micron band of ozone. *Quart. J. R. meteor. Soc.*, **87**, 562–577.

Houghton, H. G., 1954: On the annual heat budget of the northern hemisphere. *J. Meteor.*, **11**, 1–9.

Houghton, J. T., and J. S. Seeley, 1960: Spectroscopic observations of the water vapor content of the stratosphere. *Quart. J. R. meteor. Soc.*, **86**, 358–370.

Howard, J. N., D. L. Burch and D. Williams, 1955: Near-infrared transmission through synthetic atmospheres. *Geophys. Res. Papers*, No. 40, Air Force Cambridge Research Center, AFCRC-TR-55-213, 244 pp.

Inn, E. C. Y., and Y. Tanaka, 1953: Absorption coefficient of ozone in the ultra-violet and visible regions. *J. opt. Soc. Amer.*, **43**, 870–873.

——, and ——, 1956: Comparison of recently recorded ozone absorption coefficient in the visible and ultraviolet region. *Conf. on Ozone*, Armor Research Foundation, 263–268.

Johnson, F. S., 1954: The solar constant. *J. Meteor.*, **11**, 431–439.

Kaplan, L. D., 1954: The infrared spectrum of the lower stratosphere and its importance in the heat balance. *Sci. Proc. Internat. Assn. Meteor.*, 10th General Assembly, Rome. 583–592.

King, J. I. F., 1952: Line absorption and radiative equilibrium. *J. Meteor.*, **9**, 311–321.

——, 1956: Radiative equilibrium of a line-absorbing atmosphere. II. *Astrophys. J.*, **124**, 272–297.

Korb, G., J. Michalowsky and F. Möller, 1956: Investigation on the heat balance of the troposphere. Tech. Report No. 1, Contract AF61(514)-863, August, 94 pp. (OTS No. PB127016 Mi. $5.40, Ph. $15.30, obtainable from Library of Congress).

London, J., 1956: A study of the atmospheric heat balance. Final Report, Contract AF 19(122)-165, Research Div., College of Engineering, New York Univ., 99 pp. (OTS No. PB129551, Mi. $5.70, Ph. $16.80).

Manabe, S., and F. Möller, 1961: On the radiative equilibrium and heat balance of the atmosphere. *Mon. Wea. Rev.*, **89**, 503–532. [Paper A].

Mastenbrook, H. J., 1962: The vertical distribution of water vapor over Hyderabad, India, and comparison with mid-latitude distribution. NRL Report 5817, August, 14 pp.

——, 1963: Frost-point hygrometer measurements in the stratosphere and the problem of moisture contamination. *Schedule and Abstracts of Technical Papers presented at the 1963 International Symposium on Humidity and Moisture*, Washington, D. C., 35–36.

Möller, F., 1943: Labilisierung von Schichtwolken durch Strahlung. *Meteor. Z.*, **60**, 212–213.

——, and S. Manabe, 1961: Über das Strahlungsgleichgewicht in der Atmosphäre. *Z. f. Meteor.*, **15**, 3–8. [Paper B].

Murakami, T., 1962: Stratospheric wind, temperature and isobaric height conditions during the I.G.Y. period. Part I. Report No. 5, Planetary Circulation Project, Dept. of Meteorology, M.I.T. (OTS No. TID15476, Xerox $14.15).

Murgatroyd, R. J., 1960: Some recent measurements by aircraft of humidity up to 50,000 ft. in the tropics and their relationship to meridional circulation. Proc. of the Symposium on Atmospheric Ozone, Oxford, 20–25 July 1959, *IUGG Monograph No. 3*, Paris, 30.

——, P. Goldsmith and W. E. H. Hollings, 1955: Some recent measurements of humidity from aircraft up to height of about 50,000 ft over Southern England. *Quart. J. R. meteor. Soc.*, **81**, 533–537.

Murgatroyd, R. J., and R. M. Goody, 1958: Sources and sinks of energy from 30 to 90 km. *Quart. J. R. meteor. Soc.*, **84**, 225–234.

Normand, C., 1953: Atmospheric ozone and the upper-air conditions. *Quart. J. R. meteor. Soc.*, **79**, 39–50.

Palmer, C. H., Jr., 1960: Experimental transmission functions for the pure rotation band of water vapor. *J. opt. Soc. Amer.*, **50**, 1232–1242.

Ramanathan, K. R., and R. N. Kulkarni, 1960: Mean meridional distribution of ozone in different seasons calculated from umkehr observations and probable vertical transport mechanism. *Quart. J. R. meteor. Soc.*, **86**, 144–155.

Riehl, H., 1962: Radiation measurement over the Caribbean during the Autumn of 1960. *J. geophys. Res.*, **67**, 3935–3942.

Sasamori, T., 1959: The temperature effect on the absorption of 15 microns of carbon dioxide band. Sci. Rep. of the Tohoku Univ., Series 5, **11**, No. 3, 149–161.

Vigroux, E., 1953: Contributions a l'etude experimentale de l'absorption de l'ozone. *Ann. de Physique*, **8**, 709–762.

Walshaw, C. D., 1957: Integrated absorption by 9.6 μ band of ozone. *Quart. J. R. meteor. Soc.*, **83**, 315–321.

White, R. M., 1954: The counter-gradient heat flux in the stratosphere. *Tellus*, **6**, 177–179.

Yamamoto, G., 1952: On a radiation chart. *Sci. Rep. of the Tohoku Univ.*, Series 5, **4**, 9–23.

——, 1955: Radiative equilibrium of the earth's atmosphere. II. The use of Rosseland's and Chandrasekhar's means in the line absorbing case. *Sci. Rep. of the Tohoku Univ.*, Series 5, **6**, 127–136.

——, 1962: Direct absorption of solar radiation by atmospheric water vapor, carbon dioxide, and molecular oxygen. *J. atmos. Sci.*, **19**, 182–188.